Two-lattice-vibration theory for proton transfer in cubic perovskites: Barium zirconate versus potassium tantalate

Grégory Geneste

Version of Record: https://www.sciencedirect.com/science/article/pii/S0167273820305373
Manuscript_f8b4c51247300cde1e3e187e475bacea

Two-lattice-vibration theory for proton transfer in cubic perovskites: barium zirconate versus potassium tantalate.

Grégory Geneste

CEA, DAM, DIF, F-91297 Arpajon, France

Abstract

Proton transfer (PT) in proton-conducting oxides is an intrinsically quantum phenomenon, due to the very strong quantization of the OH stretching vibration ($\hbar\omega \sim 0.4$ eV). Up to high temperatures, the proton is frozen in its ground state for this vibration, and does not undergo the thermal agitation. Therefore, these are the thermal fluctuations of the (heavier) lattice atoms which make PT possible, at least above $\sim$ half the Debye temperature of the lattice. These fluctuations may occasionally and randomly produce specific lattice configurations in which the quantum protonic ground levels in the two wells are equalized (coincidence), making PT possible, however with a certain probability. An analytical expression of this transfer probability may be obtained as the solution of a curve-crossing quantum-mechanical problem, and thus described by the Landau-Zener (LZ) formula. Two lattice vibrations play a fundamental role in PT: (i) a *reorganization* of the lattice, that sends the protonated system from its initial self-trapped configuration up to the coincidence manifold, and (ii) a *reduction of the (donor) oxygen - (acceptor) oxygen distance Q*, which facilitates PT by making the system reach coincidence configurations with smaller proton barrier, and thus larger LZ probability. In cubic perovskites, the set of the coincidence configurations plays the role of the transition state for PT. The implementation of this theory of proton transfer [G. Geneste, Solid State Ionics **323**, 172 (2018)] is here strongly improved on several points: description of the coincidence configurations, proton zero-point energies and proton potential at coincidence. It is then re-applied to barium zirconate (BZO), and also to potassium tantalate (KTO), with parameters derived from density-functional theory (DFT) calculations. The theory confirms the adiabatic PT regime in BZO, common to most proton conductors, with a negligible contribution of non-adiabatic tunneling transfers to the transfer rate. In KTO, by contrast, the relative contribution of non-adiabatic tunneling transfers is much larger, especially below $\sim$ 250-300 K. The present work helps to characterize intrinsic features common to most proton conductors, at least from the point of view of proton mobility within the lattice. The activations energies for proton transfer at high temperature are predicted at 0.11 eV (BZO) and 0.25 eV (KTO).

Keywords: Proton transfer, lattice reorganization, Landau-Zener, barium zirconate, potassium tantalate

1. Introduction

Proton-conducting oxides possess strong potentialities for clean energy applications [1]. In particular, they may be used as electrolytes in Protonic Ceramic Fuel Cells (PCFCs), a class of fuel cells having a working temperature $\sim$ 600-900 K, intermediate between that of proton exchange membrane fuel cells (PEMFCs), and that of solid oxide fuel cells (SOFCs), that work at high temperature. PCFCs are promising devices because their working temperature is sufficiently high to have efficient hydrogen dissociation and good proton conductivity, but low enough to reduce materials degradation and thermal stress [1], which are a common problem at high temperature.

Among the oxide materials that can be used as electrolytes for PCFCs, several perovskites have been identified as good candidates: interesting levels of protonic conductivity have been obtained, e.g. in barium zirconate $BaZrO_3$ (BZO) [2, 3], and barium cerate $BaCeO_3$ (BCO) [3, 4], doped with trivalent elements such as Y or Gd on their B site (i.e. Zr or Ce site). In humid atmosphere, these materials undergo an hydration reaction that produces protonic defects [5], as the product of the dissociation of water molecules in the charged oxygen vacancies (that result from aliovalent doping), according to the reaction $H_2O(g) + V_O^{\bullet\bullet} + O_O^X \rightarrow 2OH_O^\bullet$. This hydration is sufficently exothermic to ensure the presence of protons in significant concentration even at the working temperatures of PCFCs. In the hydrated systems, the protons are bonded to oxygen atoms under the form of hydroxyl groups OH, that, roughly speaking, usually point along the [100] pseudo-cubic directions of the perovskite lattice.

It is now rather well admitted that protons in these materials diffuse over large distances thanks to the succession of two processes [2, 6]: (i) a reorientation (also called *rotational diffusion*), during which the OH bond rotates by an angle of about 90°, and (ii) a *transfer*, during which the covalent OH bond breaks, and H^+ jumps onto a nearest (acceptor) oxygen, usually along an hydrogen bond that may preexist between the proton and the acceptor oxygen.

However, modeling proton transfer (PT) in those systems is made complex by the quantum nature of the protonic motion. This quantum nature results from the strong quantization of the protonic vibration along the direction of stretching of the OH

bond, and in a PT process, the stretching of OH is necessarily involved. In the stable configuration of the proton, the energy quantum associated to OH stretching is $\sim$ 0.4 eV, which corresponds to a characteristic temperature of $\sim$ 4600 K. Thus, up to very high temperatures, H^+ in its stable position may be considered as frozen in the ground state of the stretching vibration. In the lattice configurations corresponding to the transition state for PT, this quantization is reduced by about one half [7]. This, however, corresponds to a characteristic temperature of $\sim$ 2000 K, indicating that, even at the working temperatures of PCFCs, strong quantum effects are expected in the PT process in proton-conducting oxides, that involves therefore mostly protonic *ground-state* contributions. *The proton is not affected by thermal fluctuations along the transfer direction within the whole working temperature regime of PCFCs.*

In a recent work [7], a theory of PT in cubic perovskites has been developed, that includes both static and dynamic quantum effects. The concepts underlying this theory are the same as those used to describe PTs in aqueous solutions [8], hydrogen interstitial hoppings in metals [9] or small polaron hoppings in insulating crystals [10]. It assumes that, since H^+ is unable to reach excited states (thermally fluctuate) in its motion along the transfer direction, the thermal energy necessary to achieve PT is provided by vibrations of the surrounding *lattice* atoms, which are sufficiently excited above half the Debye temperature T_D of the lattice [11] (typically, $T_D/2 \sim$ 150-200 K in perovskite oxides). In a PT process, these lattice vibrations may occasionally send the system to the transition state, in which transfer takes place with a certain probability. In a cubic perovskite, we may consider that this transition state is formed by a set of particular lattice configurations – the *coincidence* configurations – in which the protonic ground levels in the two wells are equal.

Thus, when the system reaches the transition state (coincidence) for PT, following thermal fluctuations of the lattice atoms, the proton may jump or not on the neighboring site, with a transfer probability P_{LZ}, that can be expressed as the result of a quantum-mechanical curve-crossing problem, using the Landau-Zener (LZ) formula [8, 7]. The thermal LZ parameter γ_{th} helps to discriminates between coincidence configurations having, on average, a small proton transfer probability ($\gamma_{th} << 1 \rightarrow \langle P_{LZ} \rangle << 1$), from the ones having, on average, a proton transfer probability close to unity ($\gamma_{th} >> 1 \rightarrow \langle P_{LZ} \rangle \sim 1$). In the former case, the transfers, when they take place, are said to be non-adiabatic and usually correspond to tunneling processes through the proton barrier. In the latter case, the transfers are said to be adiabatic and are associated, either to tunneling with a large transfer probability (proton ground state energy close to the barrier top in the proton coordinate) or to processes in which the proton ground state energy already exceeds the proton barrier at coincidence.

Two particular lattice vibrations play a fundamental role in the PT process:

- a necessary vibration: the lattice *reorganization*, which consists in transfering the self-trapping distortion from the initial site onto the final site, and can be viewed as the natural reaction coordinate for PT;
- a facilitating vibration: the reduction of the distance Q between the donor and the acceptor oxygens.

In Ref. [7], this theory was applied to PT in BZO, and the parameters feeding the theory deduced from density-functional theory (DFT) calculations. It was shown that the coincidence configurations that provide the largest contribution to the transfer rate have $\gamma_{th} > 1$, indicating that the PT regime in $BaZrO_3$ is adiabatic, down to 150-200 K. These configurations exhibit a short separation between the two oxygens involved in the transfer, typically < 2.55 Å, and thus a small PT barrier. Below a separation of 2.475 Å, the zero-point energy (ZPE) of the proton even exceeds the PT barrier, and the corresponding contributions become dominant in the transfer rate above 200 K, which is characteristic of a regime called the *adiabatic limit for PT* [12].

Moreover, we had clearly identified the nature of the reorganization in BZO: it (mostly) consists of a rotation of the oxygen octahedra by a few degrees, in the other sense as the one associated with the self-trapping distortion. Therefore in BZO, the *interoctahedral* motion associated with the reorganization and the *intraoctahedral* motion associated with the reduction of Q play complementary roles to make PT possible.

Several points however, can be improved in the implementation of this theory, and this is the first goal of the present article. In particular, the proton potential at coincidence in this new work is modeled by a 6th-order polynom (rather than 4th-order in the previous work). The parameters of this 6th-order polynomial function are then fitted, not only on the proton barrier height and width obtained by DFT, but also on the curvature of the well at its minimum. Therefore, the ZPEs of the proton at coincidence are much better described.

In a second time, this improved implementation is re-applied to barium zirconate (BZO), and also to potassium tantalate (KTO). We confirm the adiabatic proton transfer regime in BZO, which is the hallmark of a good proton conductor. In KTO, however, the relative contribution of non-adiabatic tunneling transfers is larger than in BZO at low temperature (typically below 250-300 K), indicating that KTO is probably not an as good proton conductor as BZO. By comparing the two oxides, the present work helps to characterize the intrinsic features of a *good* proton conductor.

The content of the article is as follows: first, experimental and theoretical results about proton mobility in BZO and KTO are briefly reviewed in Sec. 2. Then, the basic concepts of the theory are recalled, in their general form (Sec. 3), and restricted to a two-lattice vibration model (Sec. 4). The latter model is applied to two emblematic oxides: barium zirconate $BaZrO_3$ (BZO) and potassium tantalate $KTaO_3$ (KTO). For that, the coincidence configurations to be considered are first described and simulated by DFT (Sec. 5), then used to calculate the parameters entering the model (Sec. 6). After that, the physical quantities of interest to transfer are computed (for H^+ and D^+) and presented simultaneously for the two compounds (Secs. 7, 8, 9, 10), to exhibit very clearly the differences between the two. Several points are discussed in Sec. 11.

2. Proton mobility in barium zirconate and potassium tantalate

In this section, we first briefly review experimental and theoretical results about proton transfer in the BZO and KTO compounds. However, owing to the very large number of experimental works performed on these two systems (in particular on BZO), this section has not the pretention to be an exhaustive review. Here we simply want to give evidence for some similarities, but also for fundamental differences between PT in BZO and PT in KTO.

2.1. $BaZrO_3$

In BZO, the activation energy for proton conductivity is measured typically between 0.40 and 0.50 eV, depending on the dopant and on the dopant concentration: Bohn and Schober report an activation energy for proton mobility of 0.44 eV in 10%Y-doped BZO [13], and Babilo and Haile an activation energy of 0.47 eV in 15%Y-doped BZO [14]. Kreuer *et al* report activations energies between 0.43 and 0.50 eV in BZO depending on the dopant (Sc, In, Y, Gd) and on the dopant concentration (between 2 and 20%) [15, 2]. Iguchi *et al* report activation energies between 0.31 and 0.42 eV in Y-doped BZO depending on Y concentration (between 5 and 15%) [16]. Ahmed *et al* report an activation energy for proton conductivity of 0.4 eV in 75%In-doped BZO [17]. Gilardi *et al* report activation energies in BZO between ~ 0.4 and 0.5 eV depending on the dopant used (Sc, In, Lu, Tm, Y, Gd, 20% concentration), and slightly larger activation energies ($\geq$ 0.55 eV) for the largest dopants (Sm, Nd) [18]. There is therefore a rather broad consensus around an activation energy of ~ 0.4-0.5 eV for proton mobility in BZO.

DFT calculations show that protons in acceptor-doped perovskites are attracted (thus trapped) by the dopants, and this trapping effect may contribute to increase the activation energy for proton mobility. In BZO, this has been deeply investigated by Björketun *et al*, who computed dopant-proton association energies between -0.21 and -0.16 eV for the most common dopants (In, Y, Gd) [19], thus suggesting that almost half of the activation energy may be due to trapping by dopants. This was further confirmed by the experimental work of Yamazaki *et al* [20], who report an activation energy of 45 kJ/mol (~ 0.47 eV) below ~ 500°C in 20%Y-doped BZO, that falls to ~ 16 kJ/mol (~ 0.17 eV) at higher temperature, where protons can escape from the attraction of Y dopants. On the other hand, DFT calculations [21, 22, 7] predict for proton transfer (far from any defect) a classical energy barrier between 0.21 and 0.27 eV. Accounting for proton quantum ZPE corrections [23] leads to a decrease of 0.12 eV of this barrier [21]. The PT barrier obtained by Sundell *et al* in BZO after inclusion of these quantum effects is thus as low as 0.09 eV.

Finally, our recent modeling [7] leads to an activation energy for PT in BZO (far from any other defect) of 0.16 eV.

2.2. $KTaO_3$

In KTO, the activation energies for proton conductivity, measured at high-temperature, are significantly larger than in BZO: protons have been incorporated in KTO doped by Fe^{3+} [24, 25], Mn^{2+} [26] or Cu^{2+} [27], with activation energies for conductivity between 0.73 and 1.02 eV [28, 29]. The same kind of H/D isotope effect is observed as in many other perovskite oxides, with the activation energy for deuteron conductivity being larger than that for proton conductivity by ~ 0.03-0.06 eV [28, 29, 25, 30]. The ratio of the proton to deuteron conductivity prefactors has been measured between 0.76 and 1.36 [28, 29], thus close to unity. These observations indicate the absence of non-adiabatic tunneling regime at high-temperature, where the measurements have been performed.

DFT calculations in KTO provide a classical barrier of 0.37 eV for proton transfer (and 0.21 eV for rotational diffusion) [31, 32], which is much smaller than the experimental activation energies, as for BZO. Since these numerical values are obtained in undoped supercells (in the absence of dopants), it may be suggested that dopants probably strongly trap the protons in KTO, with trapping energies perhaps more negative than in BZO: this may be due to the fact that trivalent dopants in BZO have a -1 formal charge state, while transition metal impurities such as Fe, Mn or Cu in substitution of pentavalent Ta probably have a more negative formal charge state, and thus attract more strongly the protons.

Recent experimental works [33, 34] suggest that proton tunneling processes may play a non-negligible role in KTO at low temperature.

3. Landau-Zener curve-crossing theory for Proton Transfer in cubic perovskites

The theory has been presented in Ref. [7], to which the reader is refered for a very detailed description. Here we recall the basic ideas, necessary to understand the content of the present work. The notations of Ref. [7] are used throughout this work[1], they are summarized in the Suppl. Info. We consider the transfer of H^+ (or D^+) from an oxygen O_i (donor) to an oxygen O_f (acceptor), 1st neighbor of O_i (the two oxygens belong to the same octahedron). Note that there are four proton sites per oxygen atom. Here the initial site (bonded to oxygen O_i) is denoted as i, while the final site (bonded to oxygen O_f) is denoted as f. The O_i-O_f distance is denoted as Q.

The presence of other defects (dopant, vacancy, other proton) is not taken into account.

3.1. Adiabatic approximation in terms of protonic state

First, PT is modeled in the framework of an adiabatic approximation in term of protonic quantum state: we assume that the difference of mass between H^+ and the lattice atoms allows the proton to instantaneously adjust its state to the lattice configuration. Moreover, the proton is treated quantum-mechanically

[1] With two exceptions: (i) the proton barrier at coincidence is denoted here as v_0 (instead of V_0 in Ref. [7]), for more clarity (the capital letter V is used to denote adiabatic and diabatic surfaces, while v lowercase is used to denote the proton potential). (ii) The Q-dependent reorganization energy and pulsation are denoted here as $\mathcal{E}_S(Q)$ and $\Omega_S(Q)$ (instead of $E_S(Q)$ and $\omega_S(Q)$) to avoid confusion with the reorganization energy E_S and pulsation ω_S.

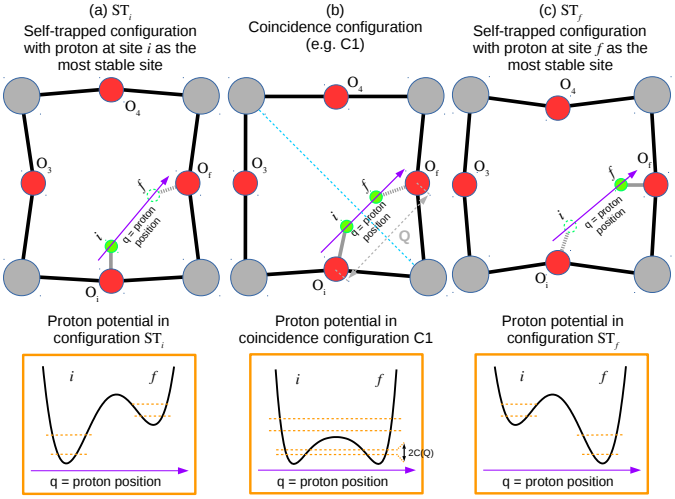

Figure 1: Schematic view of different configurations involved in an intraoctahedral proton transfer process in a cubic perovskite such as $BaZrO_3$. The transfer if from site i of ocygen O_i onto site f of oxygen O_f. (a) Self-trapped configuration ST_i: the proton is localized at site i of oxygen O_i, and the lattice relaxed around. (b) One possible coincidence (transition state) configuration (e.g. C1); (c) Self-trapped configuration ST_f: the proton is localized at site f of oxygen O_f, and the lattice relaxed around. Bottom panels: (schematic) proton potential versus proton coordinate q in these three lattice configurations, with positions of the quantum levels of the proton schematically positionned.

and the lattice classically. Denoting as $\vec{q}$ the proton position, $\vec{R}$ the lattice configuration, and $v_H(\vec{q};\vec{R})$ the potential energy of the { lattice + proton } system, the proton is considered as merged in a potential in $\vec{q}$, $v_H(\vec{q};\vec{R})$ – called *proton potential* – which parametrically depends on the lattice configuration $\vec{R}$. The quantized eigenenergies of the proton are therefore functions of $\vec{R}$ and are called *adiabatic energy surfaces*, or *adiabatic energy curves*.

For the following, it is convenient to make the approximation that the proton position along the transfer direction, q, and that perpendicular to the transfer direction, $\vec{q}_\perp$, are decoupled in the proton potential, so that $v_H(\vec{q};\vec{R})$ may be written as

$$v_H(\vec{q};\vec{R}) \approx v(q;\vec{R}) + v_\perp(\vec{q}_\perp;\vec{R}) \qquad (1)$$

It is clear that this decoupling assumption cannot be considered as correct in the stable (self-trapped) configuration of the proton. However, it is rather well justified in any coincidence configuration. Note that a one-dimensional modeling of the proton potential at coincidence was already employed in cubic perovskites by several authors [21, 35, 30].

The proton adiabatic eigenstates depend on the lattice configuration and are denoted $|\Phi^H_{nn'}\rangle(\vec{R})$. They may be written as $|\Phi^H_{nn'}\rangle(\vec{R}) = |\Phi_n\rangle(\vec{R}) \otimes |\Phi_{\perp,n'}\rangle(\vec{R})$ owing to the decoupling approximation mentioned above (n and n' are quantum numbers indexing the proton adiabatic eigenstates). The corresponding proton adiabatic eigenwavefunctions (position representation) then write $\Phi^H_{nn'}(\vec{q};\vec{R}) = \Phi_n(q;\vec{R}) \times \Phi_{\perp,n'}(\vec{q}_\perp;\vec{R})$. They parametrically depend on the lattice configuration $\vec{R}$.

Within this decoupling approximation, the strong quantization of the OH stretching vibration clearly appears when the Schrödinger equation is solved in q only,

$$-\frac{\hbar^2}{2m}\frac{d^2\Phi_n}{dq^2}(q;\vec{R}) + v(q;\vec{R})\Phi_n(q;\vec{R}) = V_n(\vec{R})\Phi_n(q;\vec{R}) \qquad (2)$$

We concentrate here on this part of the proton potential, considering that it is the one that controls PT, and ignore, at least in a first time, the possible contribution to PT of the vibration in $\vec{q}_\perp$.

The ground-state adiabatic surface is denoted as $V_{GS}(\vec{R})$ (i.e. for the ground state, the quantum number n is denoted as GS): it is thus the potential energy of the system with the lattice in configuration $\vec{R}$, and the proton in its *adiabatic* ground state $|\Phi_{GS}\rangle(\vec{R})$. Also, $V_{1st}(\vec{R})$ is the proton 1st excited state adiabatic surface, i.e. the potential energy of the system with the proton in its adiabatic 1st excited state $|\Phi_{1st}\rangle(\vec{R})$ (for the 1st excited state, the quantum number n is denoted as $1st$).

It is also convenient to introduce *diabatic energy surfaces*, which correspond to a state of the proton unambiguously localized in one of the two proton sites i or f. The diabatic ground states at sites i and f are denoted as $|\Psi_i\rangle(\vec{R})$ and $|\Psi_f\rangle(\vec{R})$. We denote $V_i(\vec{R})$ (resp. $V_f(\vec{R})$) the potential energy of the system with the lattice in configuration $\vec{R}$, and the proton in the diabatic ground state at site i (resp. f).

Owing to the strong quantization of the proton levels associated with the vibration in q (along PT direction), it is reasonable – thus within the framework of this decoupling approximation – to consider that only the two diabatic ground states are significantly populated up to rather high temperature. The transfers here considered are thus only *ground-state transfers*, i.e. transfers in which only the two proton diabatic ground states are involved.

The adiabatic approximation in terms of protonic state may be considered as true except at surface crossings where it may fail. Thus, far from surface crossings, the system evolves on the adiabatic surface $V_{GS}(\vec{R})$, which means that H^+ instantaneously adjusts its state to the adiabatic ground state $|\Phi_{GS}\rangle(\vec{R})$ associated with the current lattice configuration $\vec{R}$. The surface crossing region is the set of the lattice configurations in which the two diabatic ground states have the same energy, which corresponds to the coincidence configurations previously introduced. Thus, at coincidence, the adiabatic approximation may be true or not, which is explained hereafter (Sec. 3.4).

3.2. *Proton self-trapping*

In the most stable state of the system, the proton is trapped at one site, and the lattice relaxed around (Fig. 1 (a)): the presence of the proton induces atomic displacements. In the polarizable oxide lattice, these atomic displacements correspond to a polarization field around the proton. This contributes to stabilize the site at which H^+ is located, and thus enforce its localization.

The lattice configuration corresponding to the proton self-trapped at site i (resp. f) of oxygen O_i (resp. O_f) is denoted as ST_i (resp ST_f). Its position in the lattice configuration space is $\vec{R}_i$ (resp. $\vec{R}_f$). The proton potential in the self-trapped configuration ST_i (resp. ST_f) is thus strongly *asymmetric*, with a pronounced minimum at site i (resp. f), see Fig. 1 (a) and (c).

Obviously, when the system evolves close to a self-trapped configuration, the diabatic and adiabatic surfaces are almost equal: for $\vec{R}$ around ST_i,$V_{GS}(\vec{R}) \approx V_i(\vec{R})$. Indeed, in the very asymmetric proton potential of ST_i, the proton adiabatic ground state is localized at site i, and thus equal to the corresponding diabatic state.

3.3. Coincidence configurations

As recalled in introduction, PT takes place in specific lattice configurations – called *coincidence configurations* – in which the energy levels of H^+ in the two wells are in coincidence. This definition of the coincidence configurations should obviously be understood in terms of *diabatic* energy levels of the proton: indeed, the proton potential at coincidence is usually considered as being a symmetric function in q, and in this symmetric potential, the two diabatic ground states are coupled by the proton coupling C, see Fig. 1 (b). At coincidence, the proton coupling[2] breaks the degeneracy of the proton diabatic ground levels, so that the two first adiabatic proton levels are separated by $2C$.

There is an infinity of coincidence configurations. In the lattice configuration space, they form an hypersurface – denoted as C –, since they are defined by the crossing of the two diabatic ground state surfaces: $V_i(\vec{R}) = V_f(\vec{R})$. In particular, they may differ from one another by the donor-acceptor distance Q, and it is rather intuitive that the proton potential at coincidence – at least the proton barrier v_0 – is mainly controlled by Q. Varying this parameter, while remaining inside the coincidence hypersurface, is thus a good way to explore efficiently this manifold.

The energy of a coincidence configuration $\vec{R}$ (with the proton in its adiabatic ground state) is denoted as $E_c(\vec{R})$: $\forall \vec{R} \in C$, $E_c(\vec{R}) = V_{GS}(\vec{R})$. This function is called the *coincidence energy*. Similarly, we introduce the energy of the coincidence configuration with the proton in one of the two diabatic ground states (which, at coincidence, have the same energy), denoted as $E_c^{i=f}(\vec{R})$: $\forall \vec{R} \in C$, $E_c^{i=f}(\vec{R}) = V_i(\vec{R}) = V_f(\vec{R})$. Both are related by $E_c(\vec{R}) = E_c^{i=f}(\vec{R}) - C(\vec{R})$, with $C(\vec{R})$ the proton coupling in coincidence configuration $\vec{R}$.

3.4. Coincidence events; transfer probability at coincidence

PT is made possible only when the lattice coordinates $\vec{R}$ cross the coincidence hypersurface, which is called a *coincidence event*. Coincidence events may occasionally and randomly occur under the effect of thermal agitation of the lattice atoms. Only under such circumstances is PT possible, however with a certain probability.

In certain coincidence configurations, the adiabatic approximation we have previously postulated may break down, because the proton may not have the time to adjust its state to the adiabatic ground state. Typically this happens when the proton barrier at coincidence v_0 is large, and thus the transfer is expected to take place by tunneling through the proton barrier: if the tunneling time ($t_H \sim \hbar/2C$) is too large (weak proton coupling), the proton remains localized on one side of the symmetric barrier in q during the time scale of the coincidence, it is not in its adiabatic ground state any more (because at coincidence, this adiabatic ground state is delocalized over the two wells). The transfer probability is small, and many occurences of the coincidence event are necessary before the protonic jump takes place. The system here deviates from the adiabatic surface, and if it happens, the transfer is thus said to be *non-adiabatic* (the adiabatic approximation is temporarily lost during the coincidence time scale). If such transfers dominate in the PT rate, the regime is said to be *non-adiabatic*.

In contrast, if the lattice coordinates $\vec{R}$ cross the coincidence hypersurface in a configuration in which the proton has the time to adjust to the adiabatic ground state, the transfer is said to be *adiabatic*, because the system does not deviate from the adiabatic surface (the adiabatic approximation remains valid). This typically corresponds to an avoided crossing, i.e. the proton coupling is very large and the degeneracy of the diabatic levels at coincidence is strongly broken. If such transfers dominate in the PT rate, the regime is said to be *adiabatic*.

Quantifying the transfer probability at coincidence appears therefore as a curve-crossing quantum-mechanical problem, and a general solution (involving the non-adiabatic cases as well as the adiabatic ones and all cases inbetween) is given by the Landau-Zener (LZ) formula [36]: the transfer probability at a coincidence event writes

$$P_{LZ} = \frac{1 - e^{-\gamma}}{1 - \frac{1}{2}e^{-\gamma}}, \tag{3}$$

in which γ is the LZ parameter, defined as

$$\gamma = \frac{2\pi}{\hbar} \frac{C(\vec{R})^2}{|\frac{d}{dt}(V_i - V_f)|}. \tag{4}$$

It depends on the lattice configuration $\vec{R}$ at coincidence via the proton coupling $C(\vec{R})$, and also on the velocity with which the diabatic levels are evolving at coincidence (which is related to the velocity of the lattice coordinates, $d\vec{R}/dt$, at the coincidence event).

If coincidence occurs in a configuration of strong coupling, with sufficiently small lattice velocity (ensuring rather large coincidence timescale), γ may be large and $P_{LZ} \to 1$. In contrast, if coincidence occurs in a configuration of weak coupling, with large lattice velocity (giving short coincidence timescale), γ may be very small, and $P_{LZ} \to 0$. Note that the possible lattice velocities obey, at equilibrium, a Maxwell-Boltzmann distribution. How a given coincidence configuration *globally* behaves is thus a function of temperature, and is characterized by the *thermal* LZ parameter γ_{th} (see Sec. 6).

3.5. Transfer rate

The PT process is made possible by the thermal fluctuations of lattice atoms, that may send the system to the transition state (TS). In this TS, PT takes place with a certain probability. The transfer rate is thus obtained by application of classical Transition State Theory (TST), in which the configurations explored

[2] The proton coupling C has been also called "tunneling matrix element" and denoted as J in several works [21, 9].

are those of the lattice (the proton is not included since it is assumed in its ground state). However, classical TST assumes that the probability of jump once the TS is reached (with a positive crossing velocity) is one[3]. Here, this assumption must be modified, and the transfer probability of one replaced by the LZ tranfer probability.

In the present system, in which the initial and final proton self-trapped configurations are symmetrically equivalent (due to cubic symmetry of the perfect lattice), we may consider that the transition state configurations rigorously correspond to the coincidence configurations [7]. Thus, the transfer rate is obtained by summing the contributions from all coincidence configurations, according to

$$k^{PT} = \langle \delta(X - X^{\ddagger}) \dot{X} \theta(\dot{X}) P_{LZ}(\vec{R}, \dot{X}) \rangle_{\mathcal{R}_i}, \quad (5)$$

where X is a reaction coordinate (homogeneous to a length), that takes the value $X(\{\vec{R}\}) = X^{\ddagger}$ at the transition state (and that increases from i to f). In this last expression, δ is the Dirac function, θ the step function ($\theta(x) = 1$ for $x \geq 0$, 0 for $x < 0$), $\mathcal{R}_i$ is the initial ("reactant") region, i.e. the region of configuration space on the side of the transition state (coincidence) hypersurface that contains ST_i. $\langle ... \rangle_{\mathcal{R}_i}$ means thermal average over $\mathcal{R}_i$, i.e. $\langle ... \rangle_{\mathcal{R}_i} = \int_{\vec{R} \in \mathcal{R}_i} \int_{\vec{P}} ... \frac{e^{-\mathcal{H}_{GS}(\vec{R},\vec{P})/k_B T}}{Z_i} d\vec{R} d\vec{P}$, $Z_i = \int_{\vec{R} \in \mathcal{R}_i} \int_{\vec{P}} e^{-\mathcal{H}_{GS}(\vec{R},\vec{P})/k_B T} d\vec{R} d\vec{P}$ (partition function associated with region $\mathcal{R}_i$), and $\mathcal{H}_{GS}(\vec{R}, \vec{P}) = V_{GS}(\vec{R}) + \mathcal{T}(\vec{P})$ the (adiabatic) hamiltonian of the lattice with the proton lying in its adiabatic ground state ($\vec{P}$ denotes the vector of the conjugate momenta of the lattice positions, and $\mathcal{T}(\vec{P})$ is the kinetic energy of the lattice).

4. Two-lattice vibration (S,Q) model for proton transfer in cubic perovskites

4.1. The two lattice distortions relevant to describe PT

The most important lattice distortions in the PT process are those that extract the system from the self-trapped configuration and take it up to the coincidence hypersurface (producing a coincidence event), preferentially in a region where the transfer is the most favorable. This can be achieved by two concomittant lattice distortions: (i) a reorganization of the lattice, (ii) a reduction of the distance Q between the donor oxygen and the acceptor oxygen.

4.1.1. Lattice Reorganization; reorganization energy

The lattice *reorganization* is the set of atomic displacements that transfers the self-trapping distortion from one proton site to a neighboring one, i.e. here it is the straight path, in the lattice configuration space, from ST_i to ST_f.

We denote by $\vec{e}_S$ the unit vector along the reorganization direction, in lattice configuration space: $\vec{e}_S = \frac{\vec{R}_f - \vec{R}_i}{\|\vec{R}_f - \vec{R}_i\|}$. Starting from ST_i and displacing the atoms along $\vec{e}_S$, the symmetry of the proton potential is progressively restored, up to C0 (position in lattice configuration space $\vec{R}_{C0}$), the configuration at mid-distance between ST_i and ST_f (which is necessarily a coincidence configuration in a cubic system), in which the proton potential is perfectly symmetric.

In BZO, the lattice reorganization mostly consists in *rotations of the four oxygen octahedra* surrounding the proton site [7]. It does not significantly impact Q, and is the only lattice distortion able to restore the symmetry of the proton potential. It is thus a *necessary* step for PT. The energy necessary to bring the system from ST_i to ST_f, *without transfering the proton*, is called the *reorganization energy*, E_S. In our previous work, it was found very large in BZO, $\sim$ 0.9 eV, reflecting the strong coupling between H^+ and the lattice [7].

4.1.2. Reduction of the oxygen-oxygen distance Q

In BZO, however, the O_i-O_f distance Q in C0 is very large ($Q \approx 2.85$ Å), so that the proton barrier height and width in this configuration are extremely large: $v_0(C0) = 0.77$ eV, $2a(C0) = 1.23$ Å. C0 is thus very unfavorable to an efficient ground-state proton transfer. To permit PT, another lattice motion must take place concomittantly to the reorganization: this complementary motion is the reduction of Q: if the two oxygens O_i and O_f come closer to each other, this reduces the proton barrier height v_0, and width $2a$. This lattice motion takes the system from C0 to other coincidence configurations more favorable to transfer (with smaller proton barrier), and can be viewed as taking place inside the coincidence hypersurface. Reduction of Q is thus a *facilitating* step for PT.

We denote by C1 (position in lattice configuration space $\vec{R}_{C1}$) the lowest-energy coincidence configuration (without accounting for proton ZPE[4]), and by $\vec{e}_Q$ the unit vector along the (C0C1) direction, in lattice configuration space: $\vec{e}_Q = \frac{\vec{R}_{C1} - \vec{R}_{C0}}{\|\vec{R}_{C1} - \vec{R}_{C0}\|}$. We have: $\vec{e}_Q \perp \vec{e}_S$. Q decreases linearly with the distance along $\vec{e}_Q$ in configuration space [7].

4.2. Formalism

In the two-lattice vibration (S,Q) model, we consider that any lattice configuration $\vec{R}$ (refenced to C0, taken as origin) may be reduced to its two components along $\vec{e}_S$ and $\vec{e}_Q$: $\vec{R} = S\vec{e}_S + \lambda_Q \vec{e}_Q$. Since Q is a linear function of λ_Q [7], we rather use directly S and Q to describe the lattice configuration, i.e. $\vec{R}$ = (S,Q). The two-dimensional (S,Q) lattice configuration is schematically represented on Fig. 2, on which the main lattice configurations have been placed (ST_i, ST_f, C0, C1). Also, on this figure, the proton potential in each of these lattice configurations is schematically drawn (in the insets).

$(-S_0, Q_0)$ and (S_0, Q_0) are the coordinates of the two self-trapped configurations ST_i and ST_f in terms of (S,Q). $2S_0$ is thus the distance between the two self-trapped configurations in configuration space. S_0 can therefore be considered as a measure of the strength of the self-trapping effect in terms of

[3] Classical TST assumes no recrossing of the transition state hypersurface.

[4] C1 is indeed the lowest-energy coincidence configuration as obtained from DFT, i.e. without taking into account any proton ZPE. Accounting for these ZPEs shifts the minimum of the coincidence energy to smaller Q, see Fig. 7.

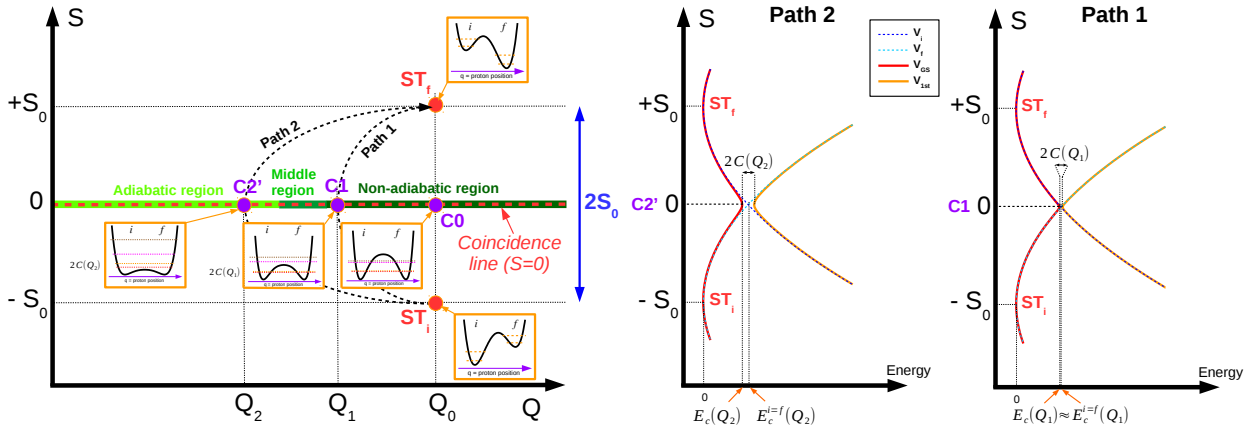

Figure 2: Schematic lattice configuration space within the present two-lattice-vibration model. The important lattice configurations (ST_i, ST_f, C0, C1, C2') are spotted with filled circles. Insets: schematic plot of the proton potential in those lattice configurations. The dashed orange lines in those insets schematically feature the proton adiabatic levels. Along the coincidence line, the proton barrier v_0 decreases as Q decreases.

magnitude of the lattice distortions. The symmetry equivalence between ST_i and ST_f in the cubic perovskite ensures that $V_f(-S,Q) = V_i(S,Q)$.

The coincidence configurations are the couples (S,Q) for which $V_i(S,Q) = V_f(S,Q)$, which here implies $V_f(S,Q) = V_f(-S,Q)$. The configurations belonging to the line defined by S=0 clearly obey this relation, and in BZO, they are the only solution physically acceptable [7]. The coincidence hypersurface C is thus here a line, defined in the (S,Q) configuration space by the cartesian equation $S = 0$ (we call it as the "coincidence line", in dashed red on Fig. 2). Along C, the different coincidence configurations depend only on Q, and thus differ from each other by the distance between the donor oxygen and the acceptor oxygen. A coincidence event corresponds to the lattice configuration crossing the coincidence line. At such event, the system may jump from a diabatic surface onto the other with a probability P_{LZ} as given by Eqs. 3 and 4. The LZ parameter γ, defined at coincidence, is thus a function of Q (through the proton coupling). It also depends on the velocity with which the diabatic levels are coming closer to each other along the motion of the lattice coordinate, when approaching the coincidence line. This velocity is obviously related to that of the lattice coordinate perpendicular to the coincidence line $\dot{S}$. The LZ parameter in this two-lattice vibration model writes

$$\gamma(Q,\dot{S}) = \frac{2\pi}{\hbar}\frac{C(Q)^2}{2|\dot{S}\frac{\partial V_i}{\partial S}(0,Q)|}, \qquad (6)$$

and P_{LZ} is therefore a function of Q and $\dot{S}$ only.

S appears as the natural reaction coordinate for PT (Fig. 2). Thus the transfer rate k^{PT} may be deduced from Eq. 5 taking S as the reaction coordinate. It finally writes as a sum over the coincidence configurations, i.e. as an integral over the coincidence line:

$$k^{PT} = \int_Q w_{out}(Q)\frac{e^{-\frac{E_c(Q)}{k_BT}}}{Z_i^{conf}}dQ. \qquad (7)$$

In this expression, Z_i^{conf} is the configurational partition function associated with region $\mathcal{R}_i$ ($S \leq 0$). It writes $Z_i^{conf} = \int_{S\leq 0}\int_Q e^{-\frac{V_{GS}(S,Q)}{k_BT}}dS\,dQ$.

The contribution to the transfer rate of the coincidence configurations with a O_i-O_f distance between Q and $Q+dQ$ is thus $w_{out}(Q)\frac{e^{-\frac{E_c(Q)}{k_BT}}}{Z_i^{conf}}dQ$. It results from a competition between two terms:

- $w_{out}(Q)$: this function is the velocity of the lattice reorganization at coincidence (thermally averaged over all possible crossing velocities), it includes the probability of successful transfer (governed by the Landau-Zener formula), and is all the more larger as Q is small;
- $\frac{e^{-\frac{E_c(Q)}{k_BT}}}{Z_i^{conf}}$: this is the occurence probability at equilibrium of the coincidence configuration considered.

The first term, the *velocity function*, writes [7]

$$w_{out}(Q) = \sqrt{\frac{2k_BT}{\pi m_S}}\int_0^{+\infty} xP_{LZ}(Q,\sqrt{\frac{2k_BT}{\pi m_S}}x)e^{-x^2}dx, \qquad (8)$$

with x in this integral being dimensionless, and $P_{LZ}(Q,\dot{S}) = \frac{1-e^{-\gamma(Q,\dot{S})}}{1-\frac{1}{2}e^{-\gamma(Q,\dot{S})}}$.

5. Self-trapped and coincidence configurations in barium zirconate and potassium tantalate from density-functional theory calculations

The theory of proton transfer presented in this work is fed with data obtained from DFT calculations.

5.1. Density-Functional Theory calculations

Our DFT calculations are performed with the ABINIT code [37], within the Generalized Gradient Approximation (GGA-PBE [38]) for the exchange-correlation energy functional, and using the Projector-Augmented Wave (PAW) framework [39, 40]. For BZO, we use the same PAW atomic data, and same numerical parameters as in Ref. [7]. All the atomic datasets are taken from the JTH table [41], except that of H (the one used here has a PAW radius of 0.8 a.u.). The plane-wave cut-off is 20 Ha in all the calculations (and 40 Ha for the double grid). The computed equilibrium lattice constants for BZO and KTO are 4.232 and 4.027 Å respectively.

Structural optimizations are performed until all cartesian components of atomic forces are lower than 1.0×10^{-5} Ha/bohr ($\sim$ 0.5 meV/Å). A 2×2×2 supercell is employed, in terms of the primitive 5-atom unit cell, in which an hydrogen interstitial in inserted (the supercell thus contains 41 atoms). Its Brillouin Zone is sampled by a 3×3×3 k-point mesh. The protonic state of H is enforced by removing one electron from the supercell, which is compensated by a uniform background. All the structural optimizations are performed with the lattice parameter and the angles of the supercell fixed, according to the theoretical GGA-PBE lattice constant.

Table 1: GGA-PBE results (energies, interatomic distances) on perfect crystals, self-trapped and coincidence configurations. Energies are in eV, distances are in Å. The reorganization energy given here is free of ZPE correction.

	$BaZrO_3$	$KTaO_3$
Lattice parameter	4.232	4.027
Self-trapped configuration ST_i		
O_iH (covalent bond)	0.986	0.981
H...O_f (hydrogen bond)	2.195	2.146
O_i-O_f	2.857	2.689
$Zr_1(Ta_1)$-$Zr_2(Ta_2)$	4.463	4.214
Proton ZPE stretching	0.209	0.214
bending1	0.052	0.052
bending2	0.042	0.047
Coincidence configurations		
C0: O_i-O_f	2.846	2.687
v_0	0.772	0.591
C1: O_i-O_f	2.610	2.581
v_0	0.236	0.354
C2: O_i-O_f	2.437	2.392
v_0	0.028	0.053
Reorganization energy E_S	0.909	0.992
Classical barrier for PT	0.258	0.362

5.2. Self-trapped configurations: ST_i and ST_f

ST_i and ST_f are obtained by structurally optimizing by DFT all the atomic positions in the system, with H^+ at site i of oxygen O_i in the first case, and at site f of oxygen O_f in the last case (these two configurations are equivalent by symmetry). First we examine these self-trapped configurations and compare BZO to KTO (Fig. 3, Tab. 1). Taking the undistorted crystal as reference, the self-trapping distortion in BZO mainly consists in rotations (by a few degrees) of the four oxygen octahedra surrounding the proton, and an increase of the distance between H^+ and the two 1st-neighbor Zr cations, as already mentioned in Ref. [7]. Obviously, the oxygen octahedra are a bit deformed as they rotate.

In KTO, this is different, the oxygen octahedra around the proton are not observed to rotate (Fig. 3). Only the 1st-neighbor Ta cations are repelled from the proton, and the oxygen O_i (to which H^+ is bonded) is pushed in the direction opposite to that in BZO. The total amplitude of the atomic distortions associated with the self-trapping effect is therefore larger in BZO than in KTO.

Despite this, the self-trapping effect is strong in both compounds, as indicated by the large reorganization energy, found around 1 eV in both cases (Tab. 1). This may be explained as follows: in BZO, the large oxygen distortions reduce O_i-O_f from 2.99 Å (perfect crystal) to 2.86 Å (ST_i), while in KTO, the motion of O_i combined with the smaller lattice parameter also reduce O_i-O_f, from 2.85 to 2.69 Å: eventually, the proton is closer from O_f and O_3 in KTO (2.15 Å) than in BZO (2.20 Å), even though the distortions in KTO are smaller.

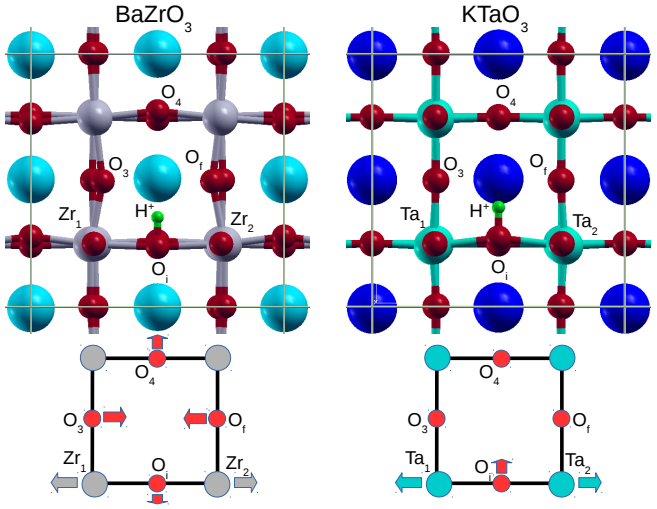

Figure 3: The self-trapped configurations in BZO and KTO. The bottom panels schematically depict the atomic distortions responsible for the self-trapping effect of the proton (they are different in the two compounds).

5.3. Coincidence configurations

5.3.1. Obtention of C0 and C1

C0 is constructed by setting the lattice atom positions at mid-distance between those of ST_i and ST_f. This is performed by first setting the centers of mass of the two configurations at the same point, to avoid the effect of undesired translations. The lattice configuration obtained is then enforced into the space group of the saddle point configuration for transfer, here *Amm*2, to eliminate the very small numerical fluctuations on the atomic positions (that come from the fact that ST_i and ST_f are optimized without symmetry constraint). The proton is then inserted in C0, close to site i at oxygen O_i, and its sole position optimized, keeping all other atomic positions as fixed. We also optimize its position in C0 at the barrier top in q (at which H^+

is maintained thanks to symmetry constraints). These two calculations provide the proton barrier height and width in lattice configuration C0.

C1 is obtained, as in Ref. [7], by a structural optimization under the constraint that the lattice keeps the symmetries of the *Amm*2 space group, while the proton remains bonded to one of the two oxygens. The proton barrier in C1 is, here again, obtained by optimizing the proton position at the top of the barrier in q (maintained thanks to symmetry constraints).

In Ref. [7], we have denoted as C2 the coincidence configuration that corresponds, for the lattice, to the geometry of the classical saddle point for transfer. Note that C0, C1 and C2 are not necessarily aligned in configuration space[5]. Thus we denote here as C2' the coincidence configuration that belongs to the (C0C1) line, and that has the same Q as C2.

5.3.2. *Improvement over Ref. [7]*

In the present work, the implementation presented in Ref. [7] is improved as follows:

- Coincidence line:

  First, in Ref. [7], we had used, for convenience, the configurations C1 and C2 as an approximation of the coincidence line (C0, C1 and C2 are almost aligned in BZO). Here we use the configurations C0 and C1, which is more conform to the general theory formulated in Ref. [7]. In BZO however, this has negligible effect on the energies and proton barriers as a function of Q at coincidence. This construction si described in Sec. 5.3.3.

- Proton potential at coincidence:

  Second, in Ref. [7], the proton potential at coincidence was modeled by a symmetric quartic double well in q, thus completely defined, in each coincidence configuration, by the proton barrier height v_0 and width $2a$, as provided by DFT calculations. However, using such a simple form, the proton zero-point energy is not well reproduced, mainly because the quartic double well does not reproduce well the curvature of the proton potential at its minima. This is improved here by using a 6th-order polynomial function in q (Sec. 5.3.4).

- Proton Zero-Point Energies:

  Third, in Ref. [7], we have made the approximation that the ZPE of the diabatic levels is the same in the self-trapped state and at coincidence (regardless of the coincidence configuration). The error induced on the energy difference between the energies of C1 and C2 was weak (at most 0.02 eV) and disfavored the adiabatic transfers. However, in the present work, this approximation is not made. The ZPE in the self-trapped state of the proton is explicitly taken into account in the calculation of the coincidence energy $E_c(Q)$ (Sec. 5.3.5).

[5] In BZO, we showed [7] that they are almost aligned, with a small angle of $\sim 11°$ between (C0C1) and (C1C2).

5.3.3. *Construction of the coincidence line; Proton barrier height and width at coincidence ($v_0(Q)$ and $2a(Q)$)*

In order to construct the coincidence line, we linearly interpolate between C0 and C1, producing several lattice configurations (26 for BZO, 36 for KTO) to exlore the coincidence line (between C0 and C1, and also beyond C1, all being regularly spaced along the coincidence line).

In each coincidence configuration, the two same DFT calculations are done as in C0 and C1, providing the proton barrier height and width. Since these configurations mainly differ from one another by Q (distance between the donor and the acceptor oxygens), we obtain, at the end, the proton barrier height, $v_0(Q)$, as well as the proton barrier width, $2a(Q)$, at coincidence, as a function of Q, . Fig. 4 displays $2a$ and v_0 at coincidence, as a function of Q. KTO and BZO exhibit a very clear difference: for a given distance Q between the two oxygen atoms, the barrier is *larger and wider* in KTO than in BZO.

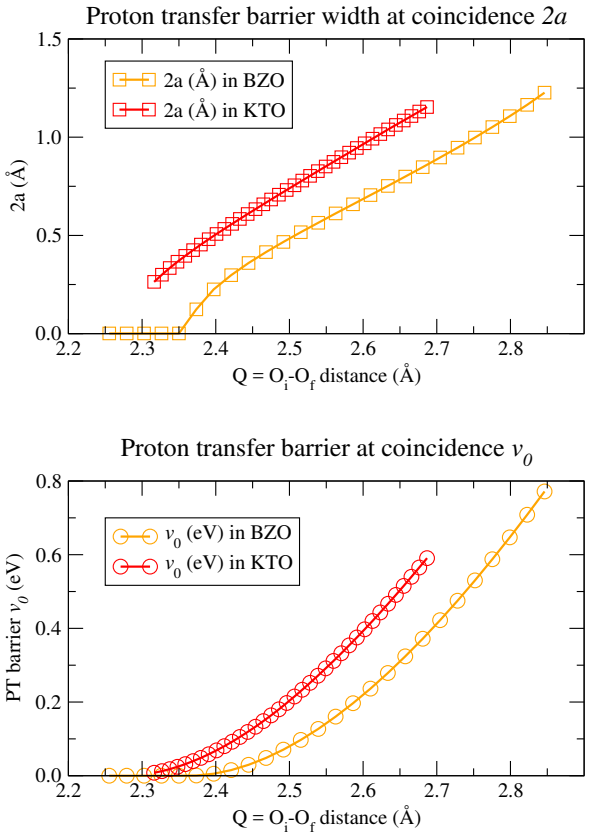

Figure 4: (Top) PT barrier width $2a$ (in Å) at coincidence as a function of (donor) oxygen - (acceptor) oxygen distance Q. (Bottom) PT barrier height v_0 (in eV) at coincidence as a function of (donor) oxygen - (acceptor) oxygen distance Q. The lines are guides for the eye.

Also, in each coincidence configuration with the proton position optimized at one of the two sites (e.g. i), six additional single-point total energy calculations are performed, by displacing manually the proton by ± 0.01 Å along the three carte-

sian directions. From these finite-difference calculations, a 3×3 force-constant matrix is constructed which, by diagonalization, provides the three force constants associated to the proton motion around the minimum of the proton potential (considering the lattice atoms as frozen).

5.3.4. *Proton potential at coincidence; Proton coupling at coincidence (C(Q))*

The proton potential at coincidence is here written under the form of a 6th-order Taylor expansion in q around q=0 [6]

$$v(q;Q) = \frac{1}{2}\alpha_2(Q)q^2 + \frac{1}{4}\alpha_4(Q)q^4 + \frac{1}{6}\alpha_6(Q)q^6 + v_0(Q) \quad (9)$$

in which the coefficients depend on Q. For each value of Q, the coefficients are fitted to reproduce exactly the proton barrier height (v_0) and width ($2a$), and the second derivative at the minimum (proton force constant) along the transfer direction (OH stretching), as obtained from DFT calculations.

However, for too small values of Q, Eq. 9 does not correspond to a double-well potential and exhibits a local minimum at q=0. Moreover, for $Q \leq 2.40$ Å in BZO and 2.32 Å in KTO, the proton potential becomes barrierless, and Eq. 9 is inadequate. We have therefore to exclude these cases. In the following, we thus restrict our study to coincidence configurations with $Q \geq 2.42$ Å in BZO (19 configurations) and 2.35 Å in KTO (33 configurations).

Then, the Schrödinger equation, which parametrically depends on Q at coincidence,

$$-\frac{\hbar^2}{2m}\frac{d^2\Phi}{dq^2}(q;Q) + v(q;Q)\Phi(q;Q) = E(Q)\Phi(q;Q) \quad (10)$$

is numerically solved, for the proton (and for the deuteron), providing, for each value of Q, the energies of the adiabatic proton (deuteron) ground state, $E_{GS}(Q)$ and adiabatic proton (deuteron) 1st excited state $E_{1st}(Q)$. Since the minimum of $v(q;Q)$ (as a function of q) is set to zero, $E_{GS}(Q)$ is the proton zero-point energy (ZPE) in the coincidence configuration having O_i-O_f distance equal to Q. The adiabatic eigenenergies at coincidence, $E_{GS}(Q)$, $E_{1st}(Q)$ are plotted as a function of Q for the proton and for the deuteron in Fig. S1 of the Suppl. Info: it can be seen that the proton ZPE, $E_{GS}(Q)$, becomes larger than the proton barrier v_0 for $Q \leq \sim 2.495$ Å[7].

The proton potential, as modeled by Eq. 9 and fitted on DFT results, is plotted in Fig. 5 for the three coincidence configurations C2', C1 and C0. The 6th-order polynom is much steeper in its repulsive part than the quartic one. Moreover, the proton ZPE in C0 is 0.19 eV, close to the ZPE in the self-trapped

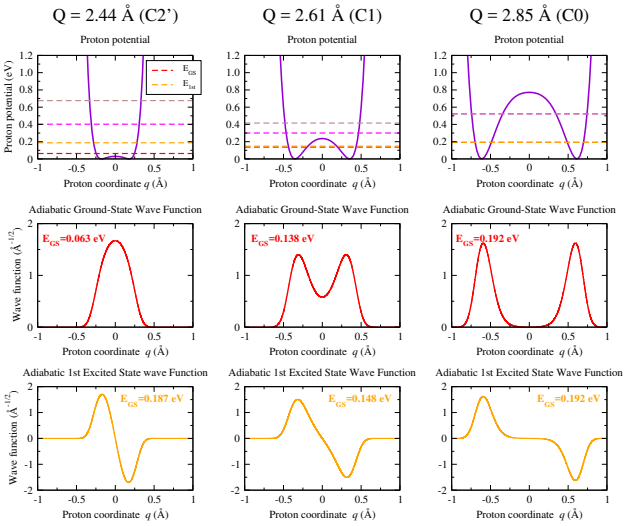

Figure 5: (Top) Proton potential (in eV) versus proton coordinate q (in Å) for the three coincidence configurations corresponding to Q=2.44 (C2'), 2.61 (C1) and 2.85 (C0) Å in $BaZrO_3$. The proton potential is modeled, according to Eq. 9, by a 6th-order polynomial function. (Middle) The three corresponding adiabatic protonic ground-state wave functions $\Phi_{GS}(q)$. (Bottom) The three corresponding adiabatic protonic 1st-excited-state wave functions $\Phi_{1st}(q)$.

state (0.21 eV, see Tab. 1), which is expected since the proton, in the C0 configuration, is strongly confined in each well. We therefore expect a more accurate description of PT by using this 6th-order polynom to model the proton potential at coincidence.

The solutions of the Schrödinger equation in each coincidence configuration are used to obtain the proton coupling at coincidence, as

$$C(Q) = [E_{1st}(Q) - E_{GS}(Q)]/2 \quad (11)$$

Fig. 6 displays the proton (and deuteron) coupling $C(Q)$ at coincidence in BZO and KTO as a function of the (donor) oxygen - (acceptor) oxygen distance Q. The function $C(Q)$ is thus known for the values of Q at which a DFT calculation has been performed. In the following however, we need to have the function $C(Q)$ regardless of the value of Q. In our previous work, we had approximated $C(Q)$ by a linear function at small Q (following Ref. [8]) and a piecewise linear function at larger Q. It would be, however, more convenient to have an approximate analytical form for $C(Q)$. According to Borgis and Hynes [8], $C(Q)$ behaves linearly at small Q and rather exponentially at large Q. These two asymptotic behaviors ($Q \rightarrow +\infty$ and $-\infty$) are well reproduced by the following function[8]

$$C(Q) \approx a_1 + a_0[ln(cosh(a_3(Q-a_2))) - a_3(Q-a_2)], \quad (12)$$

which is then used as a model for $C(Q)$: on Fig. 6, the fits by Eq. 12 are superimposed to the computed values of the proton coupling, showing satisfactory agreement between the data and the fit.

[6] note that the minimum of the proton potential at coincidence is set to zero for convenience. In the present treatment, this does not raise any problem with the fact that the diabatic energy surfaces are also fixed to zero in the self-trapped configurations, because the proton potential at coincidence is only used to extract the proton coupling, as $2C = E_{1st} - E_{GS}$ (by solving the Schrödinger equation). C thus does not depend on the absolute values of the proton eigenvalues, but only on their difference.

[7] this was 2.475 Å with the proton potential modeled by a quartic polynom [7].

[8] This functional form for $C(Q)$ has no theoretical justification in the present framework; it is just chosen because it exhibits the expected asymptotic behaviors ($Q \rightarrow +\infty$ and $-\infty$), and because it fits very well the computed values.

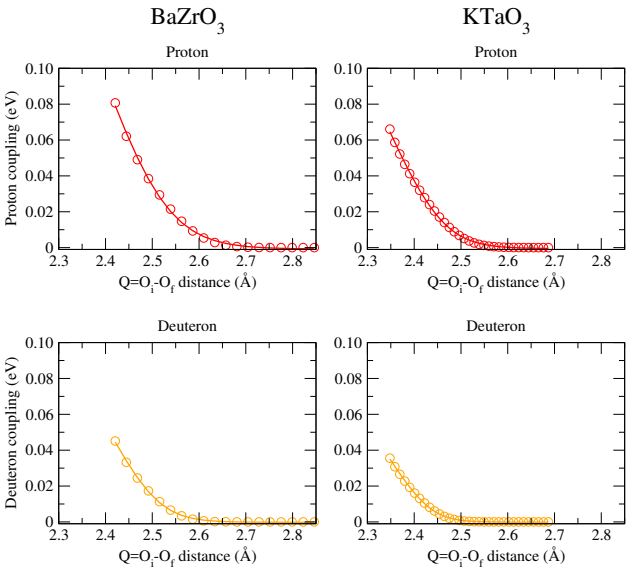

Figure 6: Proton (and deuteron) coupling at coincidence, $C(Q)$ (in eV), in BZO and KTO. $C(Q)$ is half the separation between the ground and 1st excited adiabatic proton (or deuteron) levels in the coincidence configuration for which the donor oxygen (O_i) - acceptor oxygen (O_f) distance is equal to Q. In each case, the open circles are the results of the calculation, while the continuous line is the fit by Eq. 12.

5.3.5. *Proton Zero-Point Energies; DFT computation of $E_c^{i=f}(Q)$ and of the coincidence energy $E_c(Q)$*

From the DFT computation of the coincidence configurations, we now calculate the coincidence energy $E_c(Q)$, which is the restriction of the ground-state adiabatic surface to the coincidence line ($E_c(Q) = V_{GS}(0, Q)$).

First we subtract the total energy of the self-trapped state, denotes ad $E_{tot}(STi[i])$, to the total energies of the coincidence configurations (with H^+ at one of the two minima of the proton potential), denoted herafter as $E_{tot}^{CC}(Q)$, providing a quantity[9] that we call here $E_c^{DFT}(Q)$:

$$E_c^{DFT}(Q) = E_{tot}^{CC}(Q) - E_{tot}(STi[i]) \qquad (13)$$

This energy does not include any proton ZPE. Then, the coincidence energy $E_c(Q)$ is obtained by correcting $E_c^{DFT}(Q)$ from the proton ZPE (associated with the stretching motion of OH), as

$$E_c(Q) = V_{GS}(0, Q) = E_c^{DFT}(Q) + \underbrace{E_{GS}(Q)}_{\substack{\text{ZPE of stretching}\\ \text{mode at coincidence}}} - \underbrace{E_{GS}(STi[i])}_{\substack{\text{ZPE of stretching}\\ \text{mode in self-trapped state}}} , \qquad (14)$$

in which $E_{GS}(Q)$ is the proton ZPE obtained by solving the Schrödinger in the coincidence configuration with O_i-$O_f = Q$, and $E_{GS}(STi[i])$ is the proton ZPE associated with the stretching mode in the self-trapped state, obtained in the harmonic approximation (see Tab. 1).

[9] In our previous work [7], this quantity was identified with $E_c^{i=f}(Q)$. This was an approximation based on the assumption that the proton ZPE was the same at coincidence (regardless of Q) and in the self-trapped state.

Then, the restriction of the 1st excited state adiabatic surface to the coincidence line is obtained as $V_{1st}(0, Q) = E_c(Q) + 2C(Q)$, and $E_c^{i=f}(Q)$ as

$$E_c^{i=f}(Q) = E_c(Q) + C(Q) = \frac{1}{2}(E_c(Q) + V_{1st}(0, Q)) \qquad (15)$$

The coincidence energy $E_c(Q)$, as well as the other first adiabatic surfaces (restricted to the coincidence line), are plotted on Fig. 7 as a function of Q. First it can be observed that the energy as a function of Q at coincidence (whether we considere $E_c(Q)$ or $E_c^{i=f}(Q)$) is rather soft, i.e. it does not vary a lot within a wide range of Q: in BZO, for instance, the coincidence energy E_c is ~ 0.13 eV at $Q \sim 2.65$ Å , drops at 0.08 eV at its minimum ($Q \sim 2.51$ Å) and re-increases to 0.13 eV for $Q \sim 2.42$ Å. Thus it only changes within 0.05 eV for a decrease of 0.23 Å of the value of Q. Moreover, the minimum of $E_c(Q)$ lies at rather small Q: ~ 2.51 Å in BZO and 2.54 Å in KTO. Thus, we confirm that producing coincidence configurations with rather small Q (i.e. decreasing Q inside the coincidence manifold) has not a prohibitive energy cost in the two materials at least down to ~ 2.40 Å, a fact already pointed by several authors in BZO [21, 42] and that Kreuer denoted as the *"softness of the oxygen array"* [30].

As pointed previously [7], this *softness* is probably *caused by* the proton, and *localized around* the proton. It is related to:

- the existence of the stabilizing hydrogen-bond between H^+ and the acceptor oxygen O_f,
- at least as importantly, to how the proton ZPE varies along the coincidence line.

This latter effect must be particularly emphasized: with decreasing Q, at coincidence, the proton ZPE $E_{GS}(Q)$ decreases as well (see Fig. S1 of the Suppl. Info) because the proton barrier v_0 decreases. This can be viewed as the quantum confinement of the proton decreasing with decreasing Q [43]. Fig. 5 illustrates very well this fact in BZO: from Q=2.85 (C0) down to 2.44 Å (C2'), the proton ZPE decreases from 0.19 eV down to 0.06 eV, i.e. this contributes to a stabilization of -0.13 eV between C0 and C2'. For Q=2.44 Å, the proton barrier is so small (0.03 eV in BZO) that the proton ZPE (0.06 eV) exceeds it ($E_{GS} > v_0$), and the proton ground-state wave function has its maximum at the barrier top in q, which can be viewed as the quantum confinement extended to the two sites (instead of one). Fig. 7 (bottom panels) also diplays the coincidence energy and the first excited-state adiabatic surface along the coincidence line in the case of the deuteron. We observe the isotope effect on the coincidence energy, e.g. in BZO, the minimum of $E_c(Q)$ is ~ 0.081 eV for H^+ versus ~ 0.127 eV for D^+.

6. Quadratic expansion of the diabatic energy surfaces

We now considere as valid the two-lattice vibration model previously introduced, so that any lattice configuration relevant to the PT problem may be completely defined by the two lattice coordinates S and Q.

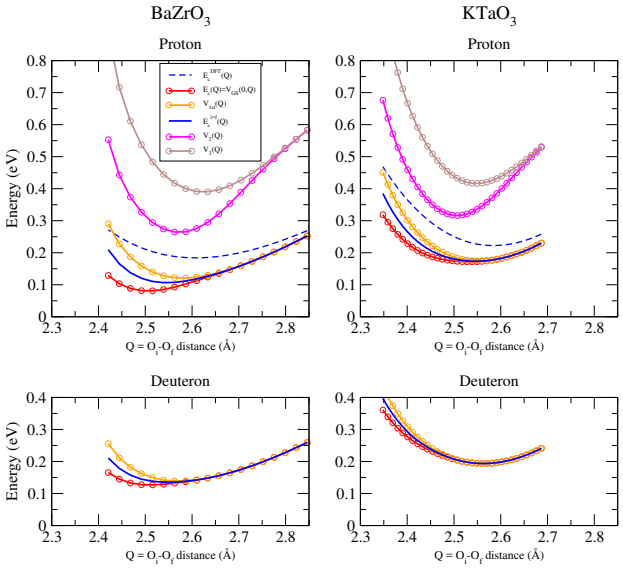

Figure 7: (Top) Adiabatic surfaces corresponding to the first proton adiabatic states (V_{GS}, V_{1st}, V_2 and V_3) cut along the coincidence line (S=0), i.e. plotted here as a function of Q, the distance between the donor and the acceptor oxygens. The restriction of V_{GS} to the coincidence line is the coincidence energy $E_c(Q)$. (Left) $BaZrO_3$; (right) $KTaO_3$. (Bottom panels) V_{GS} and V_{1st} along the coincidence line in the case of the deuteron. The lines are guides for the eye.

In order to make possible a numerical calculation of the transfer rate (Eq. 7), it is necessary to model the coincidence energy $E_c(Q)$ and the velocity function $w_{out}(Q)$ (Eq. 20). For that, the most simple is to expand quadratically the diabatic surfaces $V_i(S,Q)$ and $V_f(S,Q)$ around their minima (ST_i for V_i, ST_f for V_f), as [10]

$$V_i(S,Q) = \frac{1}{2}K_{SS}(S+S_0)^2 + \frac{1}{2}K_{QQ}(Q-Q_0)^2 + K_{SQ}(S+S_0)(Q-Q_0) \quad (16)$$

$$V_f(S,Q) = \frac{1}{2}K_{SS}(S-S_0)^2 + \frac{1}{2}K_{QQ}(Q-Q_0)^2 + K_{SQ}(-S+S_0)(Q-Q_0) \quad (17)$$

The coincidence manifold is thus defined by $V_f(\vec{R}) - V_i(\vec{R}) = -2[K_{SS}S_0 + K_{SQ}(Q-Q_0)]S = 0$, which corresponds to two lines in the (S,Q) configuration space: S=0 and $K_{SS}S_0 + K_{SQ}(Q-Q_0)$=0. Using the parameters determined by DFT hereafter, the second line corresponds to Q=2.39 Å (BZO) and 2.28 Å (KTO). We assume here that only the line S=0 is physically acceptable[11]: S=0 is thus the cartesian equation of the coincidence line. The reorganization energy is $E_S = V_i(\vec{R}_f) - V_i(\vec{R}_i) = 2K_{SS}S_0^2$.

[10] The minimal value of V_i (and V_f) is chosen to be zero. Moreover, the symmetry-equivalence between the two self-trapped configurations ST_i and ST_f imposes relationships between the coefficients of these two expansions.

[11] The other line corresponds to higher-energy configurations.

6.1. Coincidence energy and velocity function in the quadratic model

The analytical expressions for the coincidence energy and the velocity function in the present quadratic model have been derived in Ref. [7]. They are recalled in the present section.

At coincidence (S=0), the two diabatic energies V_i and V_f are equal (to $E_c^{i=f}(Q)$):

$$E_c^{i=f}(Q) = \frac{E_S}{4} + \frac{1}{2}K_{QQ}(Q-Q_0)^2 + K_{SQ}S_0(Q-Q_0) \quad (18)$$

The coincidence energy $E_c(Q)$ (= $V_{GS}(0,Q)$, restriction of the ground-state adiabatic surface to the coincidence line) is simply obtained by subtracting the proton coupling to $E_c^{i=f}(Q)$. It depends on Q only and writes:

$$E_c(Q) = \frac{E_S}{4} + \frac{1}{2}K_{QQ}(Q-Q_0)^2 + K_{SQ}S_0(Q-Q_0) - C(Q) \quad (19)$$

In this quadratic model, the velocity function writes

$$w_{out}(Q) = \sqrt{\frac{2k_BT}{\pi m_S}} \int_0^{+\infty} xP^*_{LZ}(Q,x)e^{-x^2}dx, \quad (20)$$

in which x is dimensionless, m_S is the mass associated with the reorganization coordinate [7],

$$P^*_{LZ}(Q,x) = \frac{1-e^{-\frac{\gamma_{th}(Q)}{2\sqrt{\pi}x}}}{1-\frac{1}{2}e^{-\frac{\gamma_{th}(Q)}{2\sqrt{\pi}x}}}, \quad (21)$$

and $\gamma_{th}(Q)$ is the *thermal* LZ parameter. It writes here

$$\gamma_{th}(Q) = \frac{2\pi}{\hbar\Omega_S(Q)}\sqrt{\frac{\pi}{\mathcal{E}_S(Q)k_BT}}C(Q)^2. \quad (22)$$

This expression involves a Q-dependent reorganization energy $\mathcal{E}_S(Q)$, given by[12] $\mathcal{E}_S(Q) = 2\left|K_{SS}S_0 + K_{SQ}(Q-Q_0)\right|S_0$, and a Q-dependent reorganization pulsation $\Omega_S(Q)$, defined according to[13] $\Omega_S(Q)^2 = \frac{\mathcal{E}_S(Q)}{2m_SS_0^2} = \omega_S^2\left|1+\frac{K_{SQ}(Q-Q_0)}{K_{SS}S_0}\right|$, with $\omega_S^2 = \frac{K_{SS}}{m_S}$. The reorganization frequency is $\frac{\omega_S}{2\pi}$. It can be interpreted as an upper limit for the attempt frequency of the transfer rate.

6.2. Parameterization of the quadratic model

The quadratic expansion of the diabatic surfaces involves three coefficients K_{SS}, K_{SQ} and K_{QQ}, which need to be determined. The coordinates of the two minima, ST_i and ST_f, are respectively (-S_0, Q_0) and (S_0, Q_0), they are known from the DFT computations of ST_i and ST_f. In order to determine the three forces constants K_{SS}, K_{SQ} and K_{QQ}, we proceed as in Ref. [7], i.e. we use the diabatic energy at coincidence, $E_c^{i=f}(Q)$ (obtained in Sec. 5.3.5, Eq. 15). $E_c^{i=f}(Q)$ writes as a 2nd-order

[12] The reorganization energy previously defined is the value of this function for $Q = Q_0$: $E_S = \mathcal{E}_S(Q = Q_0)$

[13] The reorganization pulsation ω_S is the value of this function for $Q = Q_0$: $\omega_S = \Omega_S(Q = Q_0)$.

polynomial function in Q within the present quadratic model (Eq. 18). The values of $E_c^{i=f}(Q)$ numerically obtained from the DFT modeling are then fitted by a 2nd-order polynom, which provides, according to Eq. 18, K_{QQ}, K_{SQ}, E_S (and thus K_{SS}). The parameters so obtained are listed in Tab. 2. Note that, since $E_c^{i=f}(Q)$ is not exactly the same for H^+ and D^+, we obtain a set of parameters for H^+, and another set for D^+.

Table 2: Parameters of the quadratic model for the proton, deduced from DFT-PBE calculations. Between [...] the parameters for the deuteron.

Parameter	BZO	KTO
S_0 (Å)	0.606	0.221
Q_0 (Å)	2.857	2.689
K_{SS} (eV/Å^2)	1.5326 [1.5271]	10.0535 [10.2551]
K_{QQ} (eV/Å^2)	4.4699 [3.7175]	8.9657 [8.0357]
K_{SQ} (eV/Å^2)	2.0029 [1.6828]	5.3937 [4.4730]
E_S (eV)*	1.1256 [1.1216]	0.9820 [1.0017]
ω_S (rad/ps)	29.528 [29.475]	62.030 [62.649]
m_S (a.m.u.)	16.96	25.21

* values from the fit of $E_c^{i=f}(Q)$ by a 2nd-order polynom.

7. Thermal Landau-Zener parameter $\gamma_{th}(Q)$

Having obtained the proton coupling at coincidence $C(Q)$, as well as the parameters describing the diabatic and adiabatic surfaces within the quadratic model, we now use these data to compute the thermal LZ parameter γ_{th} as a function of Q, according to Eq. 22. We recall that $\gamma_{th}(Q)$ is a dimensionless parameter which can be considered as a rough *criterion for adiabaticity*[14].

Let us consider a coincidence configuration with a distance Q between the donor oxygen O_i and the acceptor oxygen O_f. If $\gamma_{th}(Q)$ is sufficiently larger than one, most transfers taking place by this coincidence configuration are adiabatic, and the corresponding region of the coincidence line is called the *"adiabatic region"*; in contrast, if $\gamma_{th}(Q)$ is much smaller than one, most transfers taking place by this coincidence configuration are non-adiabatic and correspond to tunneling transfers. The corresponding region of the coincidence line is, in that case, called the *"non-adiabatic region"*. Also, there is a region of the coincidence line inbetween, in which $\gamma_{th}(Q)$ is close to unity: the transfers taking place through this region have no well-defined nature. We call it the *"middle region"*.

$\gamma_{th}(Q)$ is plotted on Fig. 8 as a function of Q (i.e. along the coincidence line), for the proton and for the deuteron in BZO and KTO.

First, we observe that, for the proton, $\gamma_{th}(Q)$ crosses 1 around 2.57 Å in BZO, versus 2.45 Å in KTO. It means that the adiabatic region is much larger in BZO than in KTO, in qualitative agreement with the proton barriers displayed in Fig. 4 being larger in KTO than in BZO for a given value of Q. For the deuteron, the same difference between the two compounds is obtained, the curves $\gamma_{th}(Q)$ being only shifted to smaller Q by $\sim$ 0.05 Å.

[14] Roughly speaking, the Q for which γ_{th}=1 corresponds to the inflexion point of the velocity function $w_{out}(Q)$.

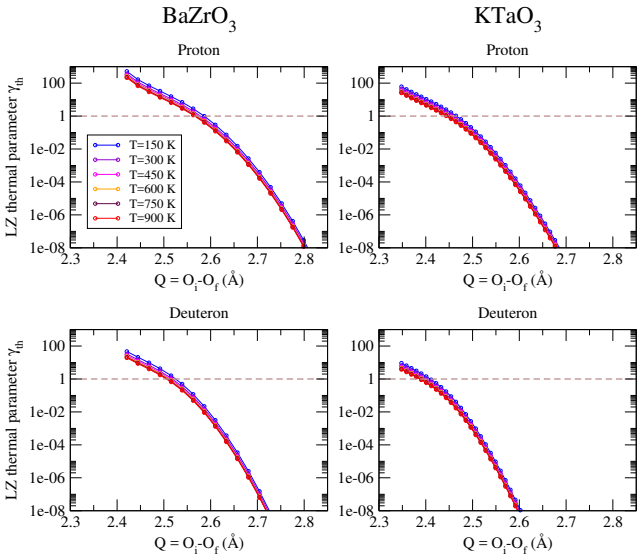

Figure 8: Thermal Landau-Zener parameter γ_{th} in $BaZrO_3$ (left panels) and $KTaO_3$ (right panels), computed for the proton (top panels) and for the deuteron (bottom panels). γ_{th} is plotted as a function of Q, the donor oxygen - acceptor oxygen distance at coincidence. γ_{th} is computed here using for the proton coupling $C(Q)$ the numerical values obtained from the resolution of Schrödinger equation (not from the fit by Eq. 12). The lines are guides for the eye.

At small Q, the expression of $\gamma_{th}(Q)$ as given by Eq. 22, may be problematic due to a cancellation of the Q-dependent reorganization energy $\mathcal{E}_S(Q)$, which leads to a divergence of $\gamma_{th}(Q)$ (for Q = 2.39 Å in BZO and 2.28 Å in KTO). However, for such small Q, the proton potential is very close to be barrierless (see Fig. 4, such small Q clearly belongs to the adiabatic region), and thus $\forall x$, $P^*_{LZ} \sim 1$. This does therefore cause no difficuly on the calculation of w_{out} and k^{PT}.

8. Velocity function $w_{out}(Q)$

We now compute the velocity function $w_{out}(Q)$ in BZO and KTO, for the proton and for the deuteron, from Eq. 20 (Fig. 9). $w_{out}(Q)$ is the velocity out of the coincidence line (through the coincidence configuration with donor-acceptor distance Q), thermally averaged over all possible incident velocities, with each incident velocity $\dot{S}$ being weighted by the LZ probability of successful crossing (Eqs. 3 and 4).

For small Q, w_{out} tends to an asymptotic non-zero value equal to $\sqrt{\frac{k_B T}{2\pi m_S}}$, that corresponds to the LZ probability equal to 1. This limit is reached in BZO for Q below $\sim$ 2.50 Å and in KTO for Q below $\sim$ 2.40 Å. In other words, in a coincidence configuration with $Q \leq$ 2.50 (resp. 2.40) Å in BZO (resp. KTO), the proton barrier v_0 is so small (and the proton coupling so large) that the vast majority of the transfers taking place by this coincidence configuration are purely adiabatic: the proton instantaneously adjusts its state to the (adiabatic) ground state (corresponding to the current proton potential), and proton transfer is automatic (P_{LZ}=1) as soon as the lattice crosses the coincidence line. The system does not deviate from the ground-state adiabatic surface. As we have said before, a regime in which such

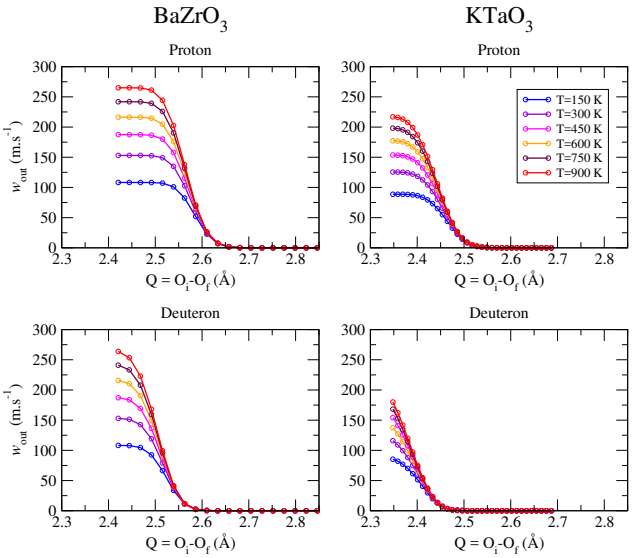

Figure 9: Velocity function $w_{out}(Q)$ in $BaZrO_3$ (left panels) and $KTaO_3$ (right panels), computed for the proton (top panels) and for the deuteron (bottom panels). The lines are guides for the eye.

configurations provide the main contribution to the transfer rate is said to be an adiabatic regime. As mentionned above, if Q is sufficiently small (below ~ 2.495 Å in BZO and ~ 2.42 Å in KTO), the proton ZPE (E_{GS}) is larger than the proton barrier v_0. If these configurations with $E_{GS} \geq v_0$ provide the main contribution to the transfer rate, proton transfer is said to take place in the *adiabatic limit* [12, 43].

For large Q, in contrast, w_{out} tends to zero, because the LZ probability tends to zero. This limit is reached in BZO for Q above ~ 2.60 Å and in KTO for Q above ~ 2.50 Å. In other words, in a coincidence configuration with $Q \geq 2.60$ (resp. 2.50) Å in BZO (resp. KTO), the proton barrier v_0 is so large (and the proton coupling so small) that the transfers taking place by this coincidence configuration, if any, are non-adiabatic and correspond to tunneling transfers: at coincidence, the proton has not the time to adjust its state to the (adiabatic) ground state (corresponding to the current proton potential), it remains in the diabatic ground state related to the initial site ($|\Psi_i\rangle$), which is localized on one side of the symmetric barrier in q. Thus the system deviates from the ground-state adiabatic surface, and proton transfer does not occur automatically at the coincidence event: it only takes place with a probablity $P_{LZ} << 1$.

In Ref. [7], we showed that the computed values of $w_{out}(Q)$ can be very well fitted by a function of the form[15] $w_{out}(Q) \approx \frac{1}{4}\sqrt{\frac{2k_BT}{\pi m_S}}[1 - tanh(A_1(T)(Q - A_2(T)))]$. This form is used hereafter to calculate the transfer rate. The parameter A_2 is very close to the value of Q for which the thermal LZ parameter equals one, while $2A_1^{-1}$ can be interpreted as the width of the middle region ($A_2 - A_1^{-1} \leq Q \leq A_2 + A_1^{-1}$). These limits vary slightly with temperature, as shown by Fig 10. Thus, we define here the three regions as follows:

- $Q \leq A_2 - A_1^{-1}$: adiabatic region;
- $A_2 - A_1^{-1} \leq Q \leq A_2 + A_1^{-1}$: middle region;
- $Q \geq A_2 + A_1^{-1}$: non-adiabatic region.

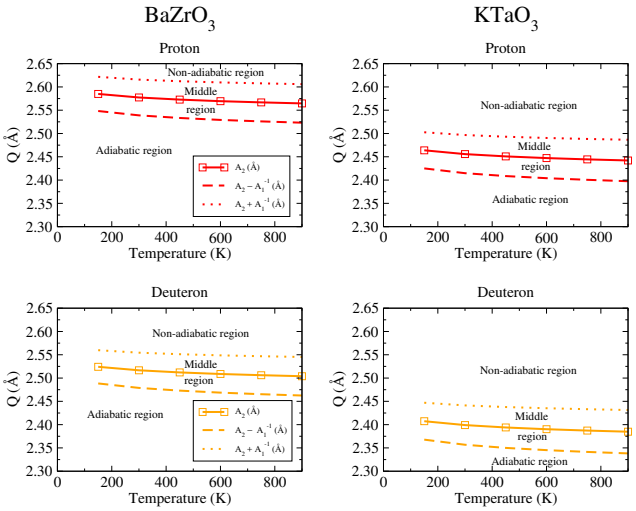

Figure 10: Temperature evolution of A_2, $A_2 - A_1^{-1}$ and $A_2 + A_1^{-1}$ in BZO (left) and KTO (right), for the proton (top) and for the deuteron (bottom). For a given temperature, the set of Q for which $Q \leq A_2 - A_1^{-1}$ is the adiabatic region of the coincidence line, the set of Q for which $A_2 - A_1^{-1} \leq Q \leq A_2 + A_1^{-1}$ is the middle region of the coincidence line, and the set of Q for which $Q \geq A_2 + A_1^{-1}$ is the non-adiabatic region of the coincidence line.

9. Contribution of each coincidence configuration to the transfer rate $W(Q)$

We now examine the function $W(Q) = w_{out}(Q)e^{-E_c(Q)/k_BT}$. $W(Q)$ is proportional to the contribution to the transfer rate of the coincidence configuration with donor oxygen O_i - acceptor oxygen O_f distance equal to Q. Its integral over the coincidence line is proportional to the transfer rate ($k^{PT} \propto \int_Q W(Q)dQ$). This function is plotted on Fig. 11 for the proton and for the deuteron, in BZO and KTO.

Let us first focus on the proton. Several differences can be observed between BZO and KTO: in BZO, the maximum of $W(Q)$ (lying around 2.45 Å) is not significantly displaced with temperature, while in KTO, it shifts to smaller Q with temperature (~ 2.48 Å at 150 K, ~ 2.42 Å at 900 K). In BZO, the largest contribution to the transfer rate comes from the adiabatic region over the whole temperature range studied, with this contribution increasing with temperature since the distribution becomes more asymetric, and spreads towards smaller Q as temperature increases. In KTO, in constrast, the largest contribution comes from the middle region. The adiabatic contribution increases with temperature but remains in minority.

[15] This functional form for $w_{out}(Q)$ has no theoretical justification in the present framework; it is just chosen because it exhibits the correct asymtotic behaviors ($Q \to +\infty$ and $-\infty$), and because we observe that it fits very well the computed values.

Transfers via the non-adiabatic region provide a non-negligible contribution at low temperature.

The origin of this difference lies in the fact that, in BZO, the minimum of $E_c(Q)$ ($\sim$ 2.51 Å), i.e. the most probable coincidence configuration, belongs to the adiabatic region, while it belongs to the non-adiabatic region in KTO ($\sim$ 2.54 Å), see Fig. 10.

In the case of the deuteron, the distributions $W(Q)$ are systematically shifted to smaller values of Q: in BZO, contributions from the middle region become more significant at low temperature, while in KTO, the non-adiabatic region provides the largest contribution at 150 K, indicating that the low-temperature transfer regime in KTO for D^+ is probably a non-adiabatic tunneling regime.

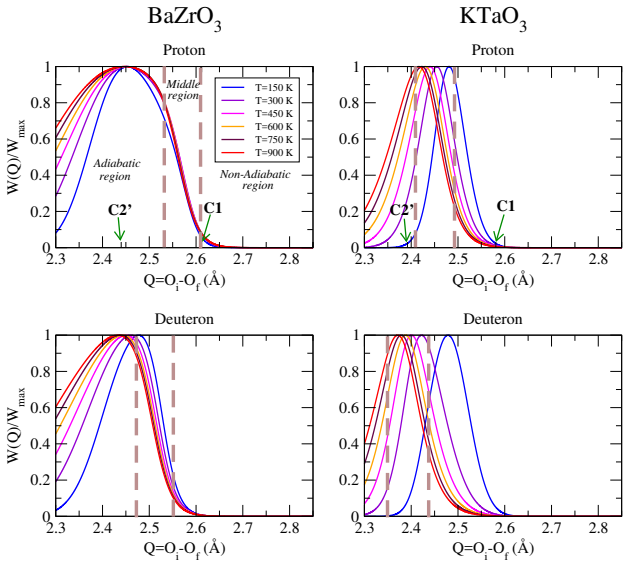

Figure 11: Function $W(Q) = w_{out}(Q)e^{-E_c(Q)/k_BT}$ (normalized by its maximal value) plotted as a function of donor oxygen O_i - acceptor oxygen O_f distance (Q). This function represents the contribution of each coincidence configuration to the transfer rate (its integral over the coincidence lines is proportional to the transfer rate: $k^{PT} \propto \int_Q W(Q)dQ$). The dashed brown vertical lines separate approximately the three regions of the coincidence line (adiabatic, middle, non-adiabatic) [they correspond here to $A_2 - A_1^{-1}$ and $A_2 + A_1^{-1}$ at 450 K and depend only slightly on temperature, see Fig. 10].

10. Transfer rate

We now compute the transfer rate k^{PT} in the two compounds, for the proton and for the deuteron, for temperatures from 150 K up to 900 K. k^{PT} is plotted in Arrhenius representation on Fig. 12.

In BZO, the transfer rate obeys an Arrhenius law, $k_L^{PT} = A_L e^{-E_L/k_BT}$ ($L = H$ and D), for both the proton and the deuteron, down to the lowest temperature here considered (150 K). The activation energy is $E_H \sim 0.09$ eV for H^+ and $E_D \sim 0.13$ eV for D^+ (Tab. 3). The prefactors are $A_H = 2.6$ THz (for H^+) and $A_D = 2.0$ THz (for D^+), a bit smaller than the reorganization frequency $\frac{\omega_S}{2\pi} = 4.7$ THz.

In KTO, the Arrhenius law is rather well obeyed in the case of the proton (activation energy $E_H = 0.18$ eV, prefactor $A_H =$

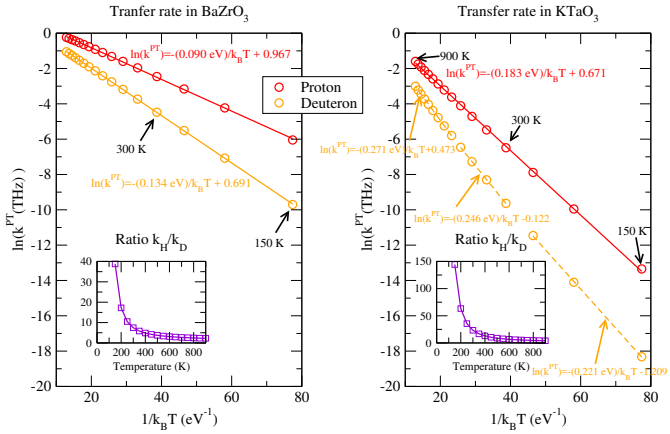

Figure 12: Transfer rate for the proton and for the deuteron in $BaZrO_3$ and in $KTaO_3$, plotted in Arrhenius representation. Insets: ratio of the proton to deuteron transfer rate as a function of temperature. The computation is made by step of 50 K.

2.0 THz), but poorly obeyed with the deuteron: we can see that the slope of the transfer rate in the case of D^+ is not the same at high temperature (activation energy $E_D \sim 0.27$ eV) and at low temperature ($E_D \sim 0.22$ eV). Also, the high-temperature prefactor for the deuteron transfer rate is $A_D \sim 1.6$ THz, significantly larger than the low-temperature prefactor ($A_D = 0.3$ THz). In contrast to BZO, the prefactors in KTO are significantly smaller than the reorganization frequency ($\sim$ 10.0 THz), indicating that non-adiabatic transfers probably play a larger role in KTO than in BZO, as anticipated in the previous section. It is probable that the transfer regime for the deuteron in KTO evolves from a non-adiabatic tunneling one at low temperature to a high-temperature regime in which contributions from configurations of the middle region dominate.

Also, the ratio of the proton to deuteron transfer rate k_H/k_D (Fig. 12, insets) is significantly larger in KTO than in BZO [16]: at 300 K, it is $\sim$ 7.5 in BZO, versus 23.3 in KTO. The ratio of the H^+ to D^+ prefactors A_H/A_D is 1.3 for BZO and 1.2 for KTO at high temperature, but 6.5 at low temperature (Tab. 3).

However, $A_H/A_D = 6.5$ is probably not sufficient to ensure that the low-temperature regime in KTO takes place in the non-adiabatic tunneling limit. Indeed, even though the relative contributions of non-adiabatic tunneling transfers to the transfer rate are much larger in KTO than in BZO, the low-temperature regime in KTO is, for the proton, dominated by contributions from the middle region rather than from the non-adiabatic one.

Following Ref. [7], we now extract the contributions to the transfer rate from coincidence configurations for which $\gamma_{th} < 1$

[16] As indicated in our previous work [7], small values of this ratio reflect the absence of non-adiabatic tunneling regime. In contrast, the large values of this ratio at low temperature are not necessarily the signature of a non-adiabatic tunneling regime, this may simply be caused by the difference of activation energies between H^+ and D^+ (related to different ZPEs for H^+ and D^+). In the latter case, inspection of the ratio of the prefactors is more significant.

Table 3: Activation energies (eV) and prefactors (THz) of the transfer rate in BZO and KTO. For BZO, the values between parenthesis are those obtained taking into account the anharmonicities of the coincidence energy, and those between brackets [...] include both anharmonicities and semi-classical corrections from bending mode ZPEs (Sec. 11.1). The reorganization frequency $\omega_S/2\pi$ (THz) is also provided.

		$BaZrO_3$	$KTaO_3$
Activation energies (eV)			
	E_H (proton)	0.090 (0.075) [0.126]	0.183
	E_D (deuteron)	0.134 (0.122) [0.159]	0.271 ($\geq$ 500 K)
			0.246 (300-450 K)
			0.221 (150-250 K)
Prefactors (THz)			
	A_H (proton)	2.63 (1.29) [1.49]	1.96
	A_D (deuteron)	2.00 (0.93) [1.03]	1.60 ($\geq$ 500 K)
			0.89 (300-450 K)
			0.30 (150-250 K)
	A_H/A_D ratio	1.32 (1.39) [1.45]	1.23 ($\geq$ 500 K)
			2.20 (300-450 K)
			6.53 (150-250 K)
Reorganization frequency $\omega_S/2\pi$ (THz)		4.7	9.9-10.0

(k_1) and from those for which $\gamma_{th} > 1$ (k_2). This is possible since the total transfer rate writes as a sum over the coincidence configurations. For that, we define Q^* as the value of Q for which $\gamma_{th} = 1$. Note that Q^* has a small dependence on temperature. We have therefore

$$k^{PT} = \underbrace{\int_{Q\geq Q^*} w_{out}(Q)\frac{e^{-\frac{E_c(Q)}{k_BT}}}{Z_i^{conf}}dQ}_{=k_1} + \underbrace{\int_{Q\leq Q^*} w_{out}(Q)\frac{e^{-\frac{E_c(Q)}{k_BT}}}{Z_i^{conf}}dQ}_{=k_2} \quad (23)$$

Fig. 13 displays k_1 and k_2 in Arrhenius representation, for the proton and the deuteron, in the two compounds. This calculation confirms that k_1 dominates over k_2 in KTO at low temperature, whereas k_2 is always larger than k_1 in BZO ($k_2/k_1 \geq 25$ for H^+ and ≥ 10 for D^+), regardless of the temperature. In KTO, there is a transition from a low-temperature regime ($k_1 > k_2$) to a high-temperature regime ($k_1 < k_2$), which takes place at $\sim$ 250-300 K for the proton, and at $\sim$ 500-550 K for the deuteron.

Finally, we also decompose k^{PT} in three contributions, according to

$$k^{PT} = \underbrace{\int_{Q\leq A_2-A_1^{-1}} w_{out}(Q)\frac{e^{-\frac{E_c(Q)}{k_BT}}}{Z_i^{conf}}dQ}_{=k_{ad}} + \underbrace{\int_{A_2-A_1^{-1}}^{A_2+A_1^{-1}} w_{out}(Q)\frac{e^{-\frac{E_c(Q)}{k_BT}}}{Z_i^{conf}}dQ}_{=k_{mid}} + \underbrace{\int_{Q\geq A_2+A_1^{-1}} w_{out}(Q)\frac{e^{-\frac{E_c(Q)}{k_BT}}}{Z_i^{conf}}dQ}_{=k_{nonad}} \quad (24)$$

k_{ad}, k_{mid} and k_{nonad} are respectively the contributions to k^{PT} of the adiabatic, middle and non-adiabatic regions of the coincidence line.

The temperature evolution of k_{ad}, k_{mid} and k_{nonad} is plotted on Fig. 14: it shows that the contribution of the adiabatic region to the transfer rate is clearly dominant in BZO, regardless of the temperature. In KTO, the middle region contribution dominates for H^+, even at the highest temperature considered here

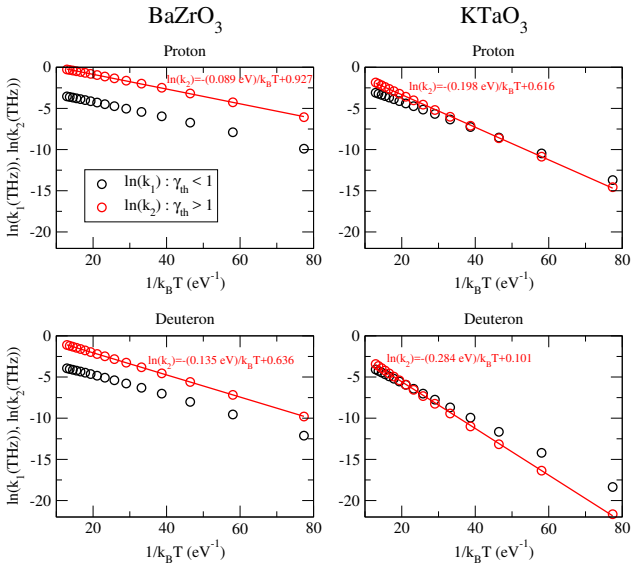

Figure 13: Arrhenius plot of k_1 and k_2 in $BaZrO_3$ and $KTaO_3$, for H^+ and D^+. k_1 (resp. k_2) is the contribution to the transfer rate from coincidence configurations for which $\gamma_{th} < 1$ (resp. $\gamma_{th} > 1$). In BZO, k_2 dominates over k_1 over the whole temperature range studied, while in KTO, there is a transition from a low-temperature regime ($k_1 > k_2$) to a high-temperature regime ($k_1 < k_2$). This transition in KTO occurs at $\sim$ 250-300 K for the proton.

(900 K), while for D^+, the middle region contribution dominates above 250 K, and the non-adiabatic contribution dominates below 250 K. This decomposition confirms that the low-temperature regime in KTO for D^+ is non-adiabatic tunneling.

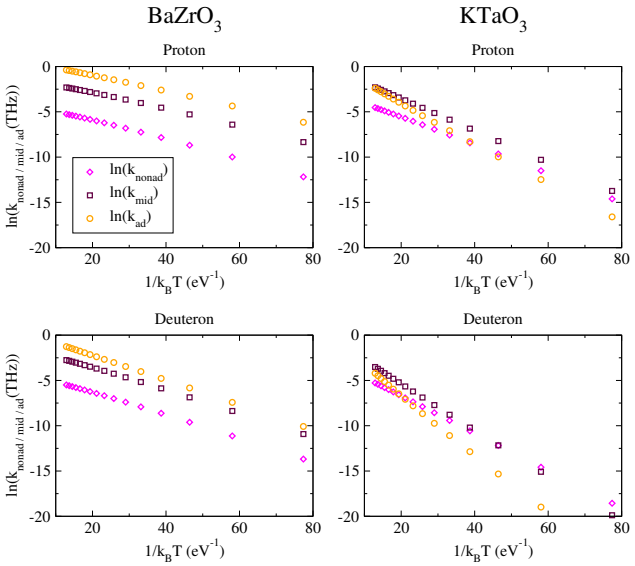

Figure 14: Arrhenius plot of k_{nonad}, k_{mid} and k_{ad} in $BaZrO_3$ and $KTaO_3$, for H^+ and D^+. k_{nonad} is the contribution to the transfer rate from the non-adiabatic region, k_{mid} is the contribution to the transfer rate from the middle region, and k_{ad} is the contribution to the transfer rate of the adiabatic region.

11. Discussion

11.1. Corrections to the model in $BaZrO_3$: anharmonicity of the coincidence energy in $BaZrO_3$, proton bending modes

The quadratic model used so far to describe the diabatic proton surfaces implies that $E_c^{i=f}(Q)$ is a 2nd-order polynom in Q. Inspection of Fig. 7 suggests that this is correct in the case in KTO, but not in BZO where $E_c^{i=f}(Q)$ (and thus also $E_c(Q)$) is rather asymetric. We therefore directly fit $E_c(Q)$ by a 4th-order polynomial function and use this polynomial expression in the calculation of the transfer rate (Eq. 7), considering however the quadratic model as valid for the calculation of the configurational partition function Z_i^{conf}[17]. The results are displayed on Fig. 15: the distribution $W(Q)$ is now found less broad, and the contribution of the "middle region" to the transfer rate is enhanced. The maximum of $W(Q)$, i.e. the configuration that provides the largest contribution to k^{PT} is also displaced up to ~ 2.50 Å. However, the contributions from coincidence configurations with $\gamma_{th} > 1$, k_2, remains largely dominant over k_1 (see Fig. S2 of the Suppl. Info). The activation energies and prefactors obtained by an Arrhenius fit are only slightly smaller than the previous ones. They are given in Tab. 3.

[17] Indeed the largest contributions to the integral Z_i^{conf} come from the region around ST_i where the function $V_{GS}(S, Q)$ is minimum and the harmonic approximation valid.

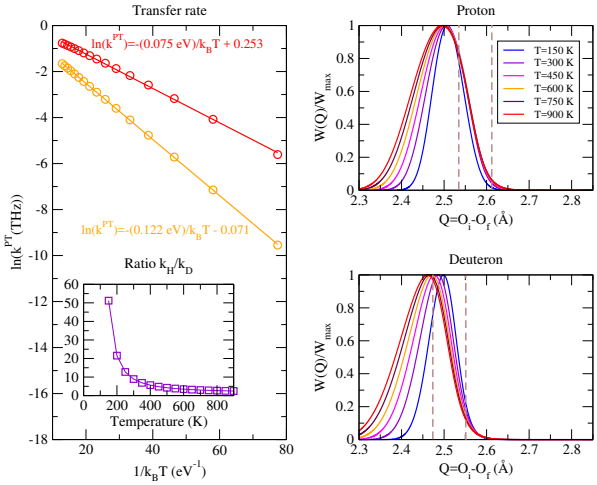

Figure 15: (Left) Transfer rate in BZO for the proton and the deuteron in Arrhenius representation, taking into account the anharmonicities of the coincidence energy. Inset: ratio of the proton to deuteron transfer rate. (Right) Function $W(Q)$ (normalized by its maximal value) plotted as a function of donor oxygen O_i - acceptor oxygen O_f distance (Q) in BZO, for H^+ (top) and D^+ (bottom). The dashed brown vertical lines separate approximately the three regions of the coincidence line (adiabatic, middle, non-adiabatic) [they correspond here to $A_2 - A_1^{-1}$ and $A_2 + A_1^{-1}$ at 450 K and depend only slightly on temperature].

We have assumed so far that the proton potential (Eq. 1) can be separated in two parts which decouple the proton coordinates q (along the transfer direction) and $\vec{q}_\perp$ (perpendicular to the transfer direction), and that only the vibration of the proton along the transfer direction (q) plays a role in the transfer process. A simple way to include the effect of the vibrations in $\vec{q}_\perp$ is to correct the energies of the coincidence and self-trapped configurations by adding the two ZPEs associated with $\vec{q}_\perp$ (thus in a semi-classical manner [21, 44]), assuming an harmonic approximation for $v_\perp(\vec{q}_\perp)$.

Note however that this semi-classical correction on the bending modes makes sense only at temperatures sufficiently lower than the characterictic temperature associated with bending mode energies, which is ~ 1000 K.

In BZO, the main effect of the ZPE of bending modes is to increase the coincidence energy by ~ 0.05 eV, because *the proton bending modes are harder at coincidence than in the self-trapped configuration* (see Fig. S3 of the Suppl. Info). Taking this new, corrected, coincidence energy in the calculation of the transfer rate (with its anharmonicity) leads to the curves of Fig. 16, in which the activation energy is found ~ 0.13 ev for H^+ and 0.16 eV for D^+ (Tab. 3).

11.2. H^+/D^+ isotope effect, test of the Swain-Schaad relationship

The present theory allows a complete modeling of the H/D isotope effect on the transfer rate. The activation energy is found larger for D^+ than for H^+ (in the two compounds), by ~ 0.03-0.05 eV, as expected. The origin lies in the ZPE, larger for the proton than for the deuteron [28, 45], that impacts the values of the coincidence energy (Eq. 14, Fig. 7).

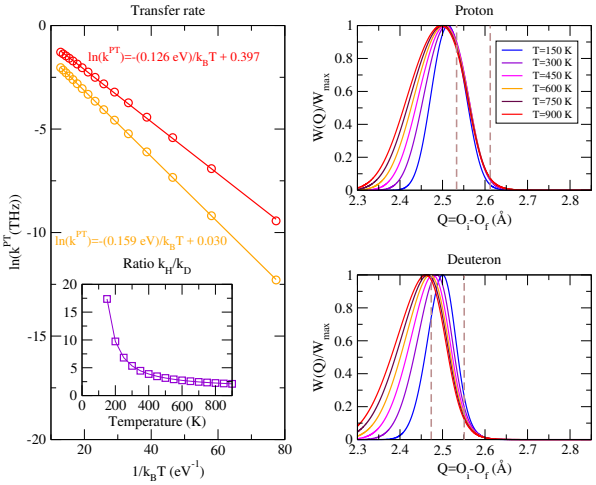

Figure 16: (Left) Transfer rate in BZO for the proton and the deuteron in Arrhenius representation, taking into account the anharmonicities of the coincidence energy, and including the proton bending modes in a semi-classical manner. Inset: ratio of the proton to deuteron transfer rate. (Right) Function $W(Q)$ (normalized by its maximal value) plotted as a function of donor oxygen O_i - acceptor oxygen O_f distance (Q) in BZO, for H^+ (top) and D^+ (bottom). The dashed brown vertical lines separate approximately the three regions of the coincidence line (adiabatic, middle, non-adiabatic) [they correspond here to $A_2 - A_1^{-1}$ and $A_2 + A_1^{-1}$ at 450 K and depend only slightly on temperature].

We also observe a slight isotope effect on the prefactor of the transfer rate, always found larger for H^+ than for D^+ ($A_H > A_D$): in BZO, the ratio A_H/A_D is $\sim$ 1.3-1.4. In KTO, this ratio is slightly larger than one (1.2) at high temperature and becomes much larger as temperature decreases (6.5 at low temperature). The origin lies in the fact that the limits separating the adiabatic, middle and non-adiabatic regions are systematically shifted to smaller Q when replacing H^+ by D^+, by $\sim$ 0.05 Å, whereas the minimum of the coincidence energy is much less affected by the isotopic substitution. Therefore, the occurence probability at coincidence, $\propto e^{-E_c(Q)/k_BT}$, overlaps less the adiabatic region for D^+ than for H^+, resulting in a smaller transfer rate and a smaller prefactor.

As indicated above, a A_H/A_D ratio close to unity may be considered as the signature of an absence of non-adiabatic tunneling regime. The increase of this ratio in KTO at low temperature reflects, in contrast, the increasing contribution of non-adiabatic tunneling transfers to the transfer rate. By scrutinizing the contribution to the transfer rate of each coincidence configuration, $W(Q)$, we have suggested in this work that a non-adiabatic (phonon-assisted) tunneling regime may be found at low temperature in KTO for D^+, whereas for H^+, configurations from the middle region rather dominate.

Here we now test the Swain-Schaad relationships [46], a set of equations sometimes used to identify the presence of a tunneling regime. The Swain-Schaad relationships are supposed to relate the transfer rates of the three hydrogen isotopes (H, D, T) when tunneling is absent. Thus any deviation from these relations should be the signature of tunneling. We use here (with obvious notations) the relationship

$$ln(k_H/k_T) = 3.3 ln(k_D/k_T) \quad (25)$$

In order to test the validity of this relationship in the present problem, we re-apply all the previous procedure for the triton T^+ (within the quadratic model of the diabatic energy surface), and calculate the triton transfer rate between 150 and 500 K[18].

The temperature evolution of the ratio $ln(k_H/k_T)/ln(k_D/k_T)$ is plotted in the Suppl. Info (Fig. S4) between 150 and 500 K. We observe that it significantly deviates from 3.3 regardless of the temperature, even in BZO where the present modeling does not give any evidence for a tunneling regime. It seems thus that the Swain-Schaad relationships are not relevant to a lattice-assisted transfer regime, i.e. Eq. 25 is not obeyed in BZO even in the absence if tunneling.

11.3. Intrinsic features of a good proton conductor

There are many conditions to fullfill for a compound to be a good proton conductor, especially in terms of capacity of hydration, trapping of the protons close to dopants and proton mobility within the lattice. We focus here on this latter point. Since the transfer rate may be written in most cases in the Arrhenius form $k_H = A_H e^{-E_H/k_BT}$, two parameters influence the proton mobility:

- The activation energy E_H;
- The prefactor A_H.

The activation energy E_H, obviously, is in relation with the coincidence energy $E_c(Q)$. The reorganization frequency $\frac{\omega_S}{2\pi}$ is an upper limit to the prefactor, because it is the attempt frequency for PT. We may thus write $A_H = \alpha_H \frac{\omega_S}{2\pi}$, with $\alpha_H \leq 1$. Using the values of Tab. 3, we have α_H = 0.27-0.56 (α_D = 0.20-0.42) in BZO, and α_H = 0.20 (α_D = 0.16 at high temperature, 0.03 at low temperature) in KTO.

In a pure adiabatic regime (and under the hypothesis of no recrossing), proton transfer would take place each time the system reaches the transition state with a positive velocity. This would give rise to $\alpha_H = 1$. The proximity of α_H to one may thus be considered as an alternative adiabaticity criterion. And indeed, α_H is smaller in KTO than in BZO. Down to $\alpha_H \sim 0.3$, as in BZO, the regime can be considered as being adiabatic, i.e. the adiabatic transfers dominate the PT rate.

Also, in a pure adiabatic regime, the activation energy E_H would be strictly equal to the minimum of $E_c(Q)$. This is rather well verified in BZO for the proton (E_H=0.075 eV using anharmonic corrections, and Min $E_c(Q)$ = 0.081 eV) and also for the deuteron (E_D=0.122 eV using anharmonic corrections, and Min $E_c(Q)$ = 0.127 eV). In fact, deviation from the adiabatic regime does not immediately break this relation, since in KTO, we have for the proton E_H=0.183 eV and Min $E_c(Q)$ = 0.172

[18]The quantization of the vibrational energy levels for T^+ is weaker than for H^+ and D^+. It is thus probable that T^+ transfer involves ground-state and excited-state transfers at moderate temperature. Thus we restrict the calculation of the triton transfer rate to temperatures lower than 500 K.

eV. However, for D^+ in KTO, we have E_D varying from 0.22 (low temperature) up to 0.27 eV (high temperature), whereas Min $E_c(Q)$ = 0.194 eV, indicating that the transfer regime in the latter case is far from being adiabatic.

As anticipated more than twenty years ago by Kreuer [47], a *good* proton conductor usually works in the adiabatic regime, with the largest contribution to the transfer rate coming from coincidence configurations with a small distance between the donor and the acceptor oxygens (typically $Q \leq 2.50$ Å), in which the proton ZPE lies above the barrier top in the proton coordinate. Indeed, an adiabatic regime ensures to have α_H as large as possible, and thus a prefactor A_H as close as possible from the reorganization frequency. From this point of view, BZO is a better proton conductor than KTO.

In order to have this adiabatic regime, typically, the minimum of $E_c(Q)$ (i.e. the saddle point configuration in the sense of the present theory) must lie within the adiabatic region, or at least, the occurence probability distribution at coincidence (which is $\propto e^{-E_c(Q)/k_BT}$), must overlap as much as possible the adiabatic region. This condition is well fullfilled in BZO, whereas it is not fullfilled in KTO (Fig. 17). It ensures that α_H is larger in BZO than in KTO.

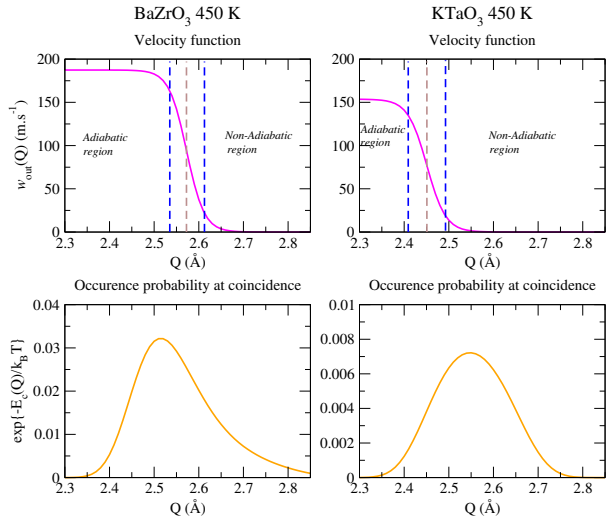

Figure 17: Comparison of the velocity function $w_{out}(Q)$ and the occurence probability at coincidence $e^{-E_c(Q)/k_BT}$, for H^+ in the two compounds at 450 K. In BZO, the occurence probability overlaps well the adiabatic region of the coincidence line, whereas this is not the case in KTO. This ensures that α_H is larger in BZO than in KTO. The dashed blue vertical lines separate approximately the three regions of the coincidence line (adiabatic, middle, non-adiabatic) [they correspond to $A_2 - A_1^{-1}$ and $A_2 + A_1^{-1}$ at 450 K and depend only slightly on temperature, the dashed brown line corresponds to A_2].

Note that however, the reorganization frequency is larger in KTO than in BZO, which compensates the smaller α_H, and the prefactors in the two compounds are finally close to each other, around 1-3 THz. In KTO, the transfer rate is smaller because of the larger coincidence energy (and thus larger activation energy).

11.4. Improving the proton barriers using the PBE0 functional

It is a well-known fact that the PBE functional underestimates proton transfer barriers. It has been shown however, that this underestimation may be strong in the gas phase, but is not so pronounced in liquids or solids [48, 49, 50]. In BZO, we showed in our previous work [7] that, by comparison with barriers obtained using the PBE0 functional [51], this underestimation varies from ~ 50% at small Q (small barriers) down to ~ 25% at large Q (larger barriers), and that the impact on the description of the transfer regime was not so drastic: we only observed a slight increase of the coincidence energy (+0.02 eV) and a slight shift of the adiabatic region (-0.01 Å), yielding a larger contribution from non-adiabatic transfers, that pushed the transition to the PT adiabatic limit to 360-370 K (instead of 250 K using PBE barriers).

Here we recompute the energy of the coincidence configurations using the PBE0 functional [51] with the VASP code [52, 53], in the framework of the present improved scheme (Sec. 5.3.2), in BZO and in KTO. As in Ref. [7], we use the geometries obtained with the PBE functional. First, as expected, we observe that the PBE0 proton barriers v_0 are larger than the PBE ones (see Fig. S5 of the Suppl. Info). The previous scheme is then completely re-applied, on BZO and KTO, based on these PBE0 proton barriers[19] (see Figs. S6, S7, S8 and S9 of the Suppl. Info). The results (activations energies and prefactors) are summarized in Tab. 4.

In both compounds, using PBE0 proton barriers slightly increases the activation energy for H^+ and D^+ transfer. In BZO, after including anharmonic corrections, the activation energy becomes E_H = 0.11 eV for the proton (and E_D = 0.16 eV for the deuteron), see Figs. S10 and S11 of the Suppl. Info. PBE0 barriers therefore increase the final activation energy by 0.03-0.04 eV only with respect to PBE ones. If the bending modes of OH are included in a semi-classical way, these energies become E_H = 0.16 eV and E_D = 0.20 eV. However, as previously explained, this correction should not be valid at the highest temperature here considered.

11.5. Symmetrization of the hydrogen bond at coincidence in the adiabatic regime

The adiabatic regime for PT in BZO mainly involves coincidence configurations with a small distance between O_i and O_f (≤ 2.50 Å), in which the proton ZPE exceeds the energy barrier in the proton coordinate ($E_{GS} \geq v_0$). This behavior corresponds to the so-called adiabatic limit for PT [12]. In these coincidence configurations with $E_{GS} \geq v_0$, the adiabatic proton ground state exhibits a single maximum at the barrier top in the proton coordinate (see Fig. 5), which means that, at coincidence, the hydrogen bond is instantaneously symmetrized.

This situation must not be confused with systems in which the hydrogen bond is symmetrized at equilibrium, such as ice

[19] The proton potential in a coincidence configuration is here determined by the PBE0 proton barrier, the PBE barrier width $2a$ and the PBE curvature at the minimum k.

Table 4: Activation energies (eV) and prefactors (THz) of the transfer rate in BZO and KTO, using PBE0 proton barriers instead of the PBE ones. For BZO, the values between parenthesis are those obtained taking into account the anharmonicities of the coincidence energy, and those between brackets [...] include anharmonicities and bending mode ZPEs (Sec. 11.1). The reorganization frequency $\omega_S/2\pi$ (THz) is also provided. Bold: the most refined values.

		$BaZrO_3$	$KTaO_3$
Activation energies (eV)			
	E_H (proton)	0.120 (**0.112**) [0.163]	**0.254**
	E_D (deuteron)	0.168 (**0.163**) [0.197]	**0.344** ($\geq$ 500 K)
			0.326 (300-450 K)
			0.305 (150-250 K)
Prefactors (THz)			
	A_H (proton)	2.08 (**1.05**) [1.13]	**2.42**
	A_D (deuteron)	1.31 (**0.76**) [0.64]	**2.29** ($\geq$ 500 K)
			1.47 (300-450 K)
			0.57 (150-250 K)
	A_H/A_D ratio	1.59 (1.39) [1.76]	1.06 ($\geq$ 500 K)
			1.65 (300-450 K)
			4.25 (150-250 K)
Reorganization frequency $\omega_S/2\pi$ (THz)		4.4-4.5	10.9-11.1

X under pressure [54, 55], or hydrogen fluoride at low temperature [56]. In these systems, the proton position lies at middistance between the two electronegative atoms, on average, indicating that even in the most stable configuration, the proton ZPE lies above the barrier top in the proton coordinate (proton self-trapping is absent).

In a proton conductor, in contrast, the proton is, most of the time, unambiguously localized at one site (self-trapping), and the hydrogen bond is only symmetrized very shortly during the transfer, when the system transits through the transision state via a coincidence configuration with short Q.

12. Conclusion

In this work, a two-lattice vibration model for proton transfer, presented in a previous work [7], has been applied to barium zirconate and potassium tantalate. Its implementation with respect to Ref. [7] is here strongly improved on several points, in particular on the description of proton ZPEs at coincidence. This allows a very accurate modeling of the coincidence energy as a function of the distance Q between the donor and the acceptor oxygens.

The proton is described as a quantum object, frozen in its vibrational ground state owing to the very strong quantization of its vibrational energy levels along the transfer direction. The proton therefore does not undergo the thermal agitation for this vibration, and proton transfer is only permitted by the thermal vibrations of the surrounding lattice atoms, which may be considered as behaving classically enough above half the Debye temperature of the lattice.

Two lattice vibrations play a role in proton transfer. The most obvious one, the reduction of the distance Q between the donor and the acceptor oxygens, is only a facilitating vibration. The necessary one is the *reorganization*, that can be defined as the vibration transferring the self-trapping distortion related to the initial self-trapped configuration onto the final site. This vibration plays the most fundamental role in the proton transfer process.

Within a simplified model in which the lattice vibrations are reduced to these two ones, the transition state for PT is a set of coincidence configurations, that mainly differ from one another by the donor-acceptor oxygen distance Q. The coincidence configurations with large Q (typically $\geq$ 2.60-2.62 Å in BZO, $\geq$ 2.50 Å in KTO) exhibit large and wide proton barriers: most transfer events occuring via such configurations are non-adiabatic tunneling (at the coincidence event, transfer only takes place with a very small probability). These lattice onfigurations form the *non-adiabatic region* of the coincidence manifold. In contrast, the coincidence configurations with small Q (typically $\leq$ 2.52-2.54 Å in BZO, $\leq$ 2.40 Å in KTO) exhibit small and narrow proton barriers: most transfer events occuring via such configurations are adiabatic. These lattice onfigurations form the *adiabatic region* of the coincidence manifold. The set of coincidence configurations lying between the non-adiabatic and the adiabatic regions is called the *middle region*.

If the most probable coincidence configuration (i.e. that of lowest energy) falls in, or close to the adiabatic region, the compound has a good chance to be a good proton conductor. Thus, whether a system behaves as a good proton conductor or not may be anticipated by comparing the velocity function with the occurrence probability distribution at coincidence. In BZO, the lowest-energy coincidence configuration corresponds to $Q \sim$ 2.51 Å, while in KTO it corresponds to $Q \sim$ 2.54 Å. Therefore, the occurence probability at coincidence overlaps well the adiabatic region in BZO, not in KTO. The transfer regime in BZO is thus adiabatic, which is usually the hallmark of a good proton conductor [47]. In KTO, the transfer rate involves significant contributions from transfers by the middle region at low temperature. The low-temperature transfer regime in KTO is thus, for the proton, intermediate between adiabatic and non-adiabatic, while it is non-adiabatic for the deuteron. Note that the larger reorganization frequency in KTO ($\sim$ 10 THz) compensates the small transfer probability within the middle region, and thus the prefactors of the transfer rate are, for the proton, similar in BZO and in KTO, around 1-3 THz.

The present implementation of the theory, including various

refinements (anharmonicity of the coincidence energy in BZO, proton barriers calculated using the PBE0 functional), predicts activation energies for PT of 0.11 eV in BZO, and 0.25 eV in KTO. The corresponding prefactors of the transfer rate are 1.0 THz in BZO, and 2.4 THz in KTO. These values must be understood as describing PT far from dopants in the two materials. Indeed, the presence of negative dopants creates a trapping effect that contributes to increase the PT activation energy with respect to the values given above [20].

Finally, we add that a complete theory of proton mobility should also include a quantitative modeling of the reorientation (rotational diffusion) motion, and of the trapping by dopants.

13. Acknowledgments

Fig. 3 has been done with the XCRYSDEN software [57].

[1] J. Kim, S. Sendogan, S. Kim, O. Kwon, Y. Bu, G. Kim, Renewable and Sustainable Energy Reviews **109**, 606-618 (2019).
[2] K.-D. Kreuer, Ann. Rev. Mater. Res. **33**, 333 (2003).
[3] E. C. C. De Souza, R. Muccillo, Materials Research **13**, 385 (2010).
[4] W. Zajac, D. Rusinek, K. Zheng, J. Molenda, Cent. Eur. J. Chem. **11**, 471-484 (2013).
[5] R. Oesten, R. A. Huggins, Ionics **1**, 427 (1995).
[6] Y. Meng, J. Gao, Z. Zhao, J. Amoroso, J. Tong, K. S. Brinkman, J. Mater. Sci. **54**, 9291 (2019).
[7] G. Geneste, Solid State Ionics **323**, 172-202 (2018).
[8] D. Borgis, J. T. Hynes, J. Phys. Chem. **100**, 1118-1128 (1996).
[9] A. Klamt, H. Teichler, Phys. Stat. Sol. **134**, 533 (1986).
[10] A. L. Shluger, A. M. Stoneham, J. Phys.: Cond. Matt. **5**, 3049 (1993).
[11] A. Klamt, "Quantum diffusion above $\Theta_{Debye}/2$", in Quantum Aspects of Molecular Motions in Solids, pp 177-181. Springer Proceedings in Physics book series (SPPHY, volume 17).
[12] P. M. Kiefer, J. T. Hynes, Solid State Ionics **168**, 219 (2004).
[13] H. G. Bohn, T. Schober, J. Am. Ceram. Soc. **83**, 768 (2000).
[14] P. Babilo, S. M. Haile, J. Am. Ceram. Soc. **88**, 2362 (2005).
[15] K.-D. Kreuer, St. Adams, W. Münch, A. Fuchs, U. Klock, J. Maier, Solid State Ionics **145**, 295 (2001).
[16] F. Iguchi, N. Sata, T. Tsurui, H. Yugami, Solid State Ionics **178**, 691 (2007).
[17] I. Ahmed, S.-G. Eriksson, E. Ahlberg, C. S. Knee, P. Berastegui, L.-G. Johansson, H. Rundlöf, M. Karlsson, A. Matic, L. Börjesson, D. Engberg, Solid State Ionics **177**, 1395 (2006).
[18] E. Gilardi, E. Fabbri, L. Bi, J. L. M. Rupp, T. Lippert, D. Pergolesi, E. Traversa, J. Phys. Chem. C **121**, 9739 (2017).
[19] M. E. Björketun, P. G. Sundell, G. Wahnström, Phys. Rev. B **76**, 054307 (2007).
[20] Y. Yamazaki, F. Blanc, Y. Okuyama, L. Buannic, J. C. Lucio-Vega, C. P. Grey, S. M. Haile, Nature **12**, 647 (2013).
[21] P. G. Sundell, M. E. Bjorketun and G. Wahnström, Phys. Rev. B **76**, 094301 (2007).
[22] N. Bork, N. Bonanos, J. Rossmeisl, T. Vegge, Phys. Rev. B **82**, 014103 (2010).
[23] K. W. Kehr, "Theory of the diffusion of hydrogen in metals", in "Hydrogen in Metals I: Basic Properties"', Topics in Applied Physics, Vol. 28, edited by G. Alefeld and J. Völkl (Springer-Verlag, Berlin, 1978), Chap.8.
[24] T. Sherban, S. Q. Fu, A. S. Nowick, MRS Proceedings **210**, 663 (1990).
[25] T. Sherban, A. S. Nowick, L. A. Boatner, M. M. Abraham, Appl. Phys. A **55**, 324 (1992).
[26] S. Q. Fu, W.-K. Lee, A. S. Nowick, L. A. Boatner, M. M. Abraham, J. Solid State Chem. **83**, 221 (1989).
[27] W.-K. Lee, A. S. Nowick, L. A. Boatner, Adv. Ceramics **23**, 387 (1987).
[28] A. S. Nowick, A. V. Vaysleyb, Solid State Ionics **97**, 17-26 (1997).
[29] W.-K. Lee, A. S. Nowick, Solid State Ionics **18-19**, 989 (1986).
[30] K.-D. Kreuer, A. Fuchs, J. Maier, Solid State Ionics **77**, 157-162 (1995).
[31] M. A. Gomez, S. Jindal, K. M. Fletcher, L. S. Foster, N. D. A. Addo, D. Valentin, C. Ghenoiu, A. Hamilton, J. Chem. Phys. **126**, 194701 (2007).
[32] S. G. Kang, D. S. Sholl, J. Chem. Phys. **141**, 024707 (2014).
[33] E. J. Spahr, L. Wen, M. Stavola, L. A. Boatner, L. C. Feldman, N. H. Tolk, G. Lüpke, Phys. Rev. Letters **102**, 075506 (2009).
[34] A. Sakurai, K. Ando, S. Ashihara, J. Chem. Phys. **149**, 104502 (2018).
[35] T. Tomoyose, N. Shimoji, K. Wakamura, J. Phys. Soc. Jpn. **74**, 3011 (2005).
[36] C. Zener, Proc. Roy. Soc. **A 137**, 696 (1932).
[37] X. Gonze, F. Jollet *et al.*, Computer Physics Communications **205**, 106 (2016).
[38] J. P. Perdew, K. Burke, and M. Ernzerhof, Phys. Rev. Lett. **77**, 3865 (1996).
[39] P. E. Blöchl, Phys. Rev. B **50**, 17953 (1994).
[40] Marc Torrent, François Jollet, François Bottin, Gilles Zérah and Xavier Gonze, Comput. Mat. Sci., **42** (2008), 337-351.
[41] F. Jollet, M. Torrent, N. Holzwarth, Comput. Phys. Comm. **185**, 1246 (2014).
[42] B. Merinov, W. Goddard III, J. Chem. Phys. **130**, 194707 (2009).
[43] G. Geneste, J. Hermet, G. Dezanneau, Phys. Chem. Chem. Phys. **19**, 21191 (2017).
[44] J. P. Bothma, J. B. Gilmore, R. H. McKenzie, New Journal of Physics **12**, 055002 (2010).
[45] N. Bonanos, A. Huijser, F. W. Poulsen, Solid State Ionics **275**, 9-13 (2015).
[46] C. G. Swain, E. C. Stivers, J. F. Reuwer Jr, L. J. Schaad, J. Am. Chem. Soc. **80**, 5885 (1958).
[47] K.-D. Kreuer, Chem. Mater. **8**, 610-641 (1996).
[48] X.-Z. Li, M. I. J. Probert, A. Alavi, A. Michaelides, Phys. Rev. Letters **104**, 066102 (2010).
[49] J. Chen, X.-Z. Li, Q. Zhang, A. Michaelides, E. Wang, Phys. Chem. Chem. Phys. **15**, 6344 (2013).
[50] A. Hassanali, F. Giberti, J. Cuny, T. D. Kühne, M. Parrinello, PNAS **110**, 13723 (2013). See the supporting Information.
[51] C. Adamo, V. Barone, J. Chem. Phys. **110**, 6158 (1999).
[52] G. Kresse and J. Hafner, Phys. Rev. B **47**, 558 (1993); **49**, 14251 (1994); G. Kresse and J. Furthmüller, Comput. Mater. Sci. **6**, 15 (1996); Phys. Rev. B **54**, 11169 (1996).
[53] G. Kresse and D. Joubert, ibid. **59**, 1758 (1999).
[54] M. Benoit, D. Marx, M. Parrinello, Nature **392**, 258 (1998).
[55] Y. Bronstein, P. Depondt, F. Finocchi, A. M. Saitta, Phys. Rev. B **89**, 214101 (2014).
[56] H. Dammak, F. Brieuc, G. Geneste, M. Torrent, M. Hayoun, Phys. Chem. Chem. Phys. **21**, 3211-3217 (2019).
[57] A. Kokalj, Comp. Mater. Sci. **28**, 155 (2003). Code available from http://www.xcrysden.org/.